phosphorylation state of Ser-129 in human alpha-synuclein determines neurodegeneration in a rat model of Parkinson disease. *Proc. Natl Acad. Sci. USA* **105**, 763–768.

Harada T., Harada C., Wang Y. L. *et al.* (2004) Role of ubiquitin carboxy terminal hydrolase-L1 in neural cell apoptosis induced by ischemic retinal injury in vivo. *Am. J. Pathol.* **164**, 59–64.

Kabuta T. and Wada K. (2008) Insights into links between familial and sporadic Parkinson's disease: physical relationship between UCH-L1 variants and chaperone-mediated autophagy. *Autophagy* **4**, 827–829.

Kabuta T., Furuta A., Aoki S., Furuta K. and Wada K. (2008a) Aberrant interaction between Parkinson's disease-associated mutant UCH-L1 and the lysosomal receptor for chaperone-mediated autophagy. *J. Biol. Chem.* **283**, 23731–23738.

Kabuta T., Setsuie R., Mitsui T., Kinugawa A., Sakurai M., Aoki S., Uchida K. and Wada K. (2008b) Aberrant molecular properties shared by familial Parkinson's disease-associated mutant UCH-L1 and carbonyl-modified UCH-L1. *Hum. Mol. Genet.* **17**, 1482–1496.

Kirik D., Rosenblad C., Burger C., Lundberg C., Johansen T. E., Muzyczka N., Mandel R. J. and Bjorklund A. (2002) Parkinson-like neurodegeneration induced by targeted overexpression of alpha-synuclein in the nigrostriatal system. *J. Neurosci.* **22**, 2780–2791.

Kirik D., Annett L. E., Burger C., Muzyczka N., Mandel R. J. and Bjorklund A. (2003) Nigrostriatal alpha-synucleinopathy induced by viral vector-mediated overexpression of human alpha-synuclein: a new primate model of Parkinson's disease. *Proc. Natl Acad. Sci. USA* **100**, 2884–2889.

Kruger R., Kuhn W., Muller T., Woitalla D., Graeber M., Kosel S., Przuntek H., Epplen J. T., Schols L. and Riess O. (1998) Ala30Pro mutation in the gene encoding alpha-synuclein in Parkinson's disease. *Nat. Genet.* **18**, 106–108.

Kurihara L. J., Kikuchi T., Wada K. and Tilghman S. M. (2001) Loss of Uch-L1 and Uch-L3 leads to neurodegeneration, posterior paralysis and dysphagia. *Hum. Mol. Genet.* **10**, 1963–1970.

Larsen C. N., Price J. S. and Wilkinson K. D. (1996) Substrate binding and catalysis by ubiquitin C-terminal hydrolases: identification of two active site residues. *Biochemistry* **35**, 6735–6744.

Larsen C. N., Krantz B. A. and Wilkinson K. D. (1998) Substrate specificity of deubiquitinating enzymes: ubiquitin C-terminal hydrolases. *Biochemistry* **37**, 3358–3368.

Leroy E., Boyer R., Auburger G. *et al.* (1998) The ubiquitin pathway in Parkinson's disease. *Nature* **395**, 451–452.

Li W., Lesuisse C., Xu Y., Troncoso J. C., Price D. L. and Lee M. K. (2004) Stabilization of alpha-synuclein protein with aging and familial Parkinson's disease-linked A53T mutation. *J. Neurosci.* **24**, 7400–7409.

Liu Y., Fallon L., Lashuel H. A., Liu Z. and Lansbury P. T. Jr (2002) The UCH-L1 gene encodes two opposing enzymatic activities that affect alpha-synuclein degradation and Parkinson's disease susceptibility. *Cell* **111**, 209–218.

Lo Bianco C., Ridet J. L., Schneider B. L., Deglon N. and Aebischer P. (2002) Alpha-synucleinopathy and selective dopaminergic neuron loss in a rat lentiviral-based model of Parkinson's disease. *Proc. Natl Acad. Sci. USA* **99**, 10813–10818.

Lombardino A. J., Li X. C., Hertel M. and Nottebohm F. (2005) Replaceable neurons and neurodegenerative disease share depressed UCHL1 levels. *Proc. Natl Acad. Sci. USA* **102**, 8036–8041.

Lowe J., McDermott H., Landon M., Mayer R. J. and Wilkinson K. D. (1990) Ubiquitin carboxyl-terminal hydrolase (PGP 9.5) is selectively present in ubiquitinated inclusion bodies characteristic of human neurodegenerative diseases. *J. Pathol.* **161**, 153–160.

Mandir A. S., Przedborski S., Jackson-Lewis V., Wang Z. Q., Simbulan-Rosental C. M., Smulson M. E., Hoffman B. E., Guastella D. B., Dawson V. L. and Dawson T. M. (1999) Poly(ADP-ribose) polymerase activation mediates 1-methyl-4-phenyl-1,2,3,6-tetrahydropyridine (MPTP)-induced parkinsonism. *Proc. Natl Acad. Sci. USA* **96**, 5774–5779.

Miura H., Oda K., Endo C., Yamazaki K., Shibasaki H. and Kikuchi T. (1993) Progressive degeneration of motor nerve terminals in GAD mutant mouse with hereditary sensory axonopathy. *Neuropathol. Appl. Neurobiol.* **19**, 41–51.

Mosharov E. V., Staal R. G., Bove J. *et al.* (2006) Alpha-synuclein overexpression increases cytosolic catecholamine concentration. *J. Neurosci.* **26**, 9304–9311.

Nishikawa K., Li H., Kawamura R. *et al.* (2003) Alterations of structure and hydrolase activity of parkinsonism-associated human ubiquitin carboxyl-terminal hydrolase L1 variants. *Biochem. Biophys. Res. Commun.* **304**, 176–183.

Nishioka K., Hayashi S., Farrer M. J. *et al.* (2006) Clinical heterogeneity of alpha-synuclein gene duplication in Parkinson's disease. *Ann. Neurol.* **59**, 298–309.

Norris E. H., Giasson B. I., Hodara R., Xu S., Trojanowski J. Q., Ischiropoulos H. and Lee V. M. (2005) Reversible inhibition of alpha-synuclein fibrillization by dopaminochrome-mediated conformational alterations. *J. Biol. Chem.* **280**, 21212–21219.

Oda K., Yamazaki K., Miura H., Shibasaki H. and Kikuchi T. (1992) Dying back type axonal degeneration of sensory nerve terminals in muscle spindles of the gracile axonal dystrophy (GAD) mutant mouse. *Neuropathol. Appl. Neurobiol.* **18**, 265–281.

Osaka H., Wang Y. L., Takada K. *et al.* (2003) Ubiquitin carboxy-terminal hydrolase L1 binds to and stabilizes monoubiquitin in neuron. *Hum. Mol. Genet.* **12**, 1945–1958.

Polymeropoulos M. H., Lavedan C., Leroy E. *et al.* (1997) Mutation in the alpha-synuclein gene identified in families with Parkinson's disease. *Science* **276**, 2045–2047.

Ramirez A., Heimbach A., Grundemann J. *et al.* (2006) Hereditary parkinsonism with dementia is caused by mutations in ATP13A2, encoding a lysosomal type 5 P-type ATPase. *Nat. Genet.* **38**, 1184–1191.

Saigoh K., Wang Y. L., Suh J. G. *et al.* (1999) Intragenic deletion in the gene encoding ubiquitin carboxy-terminal hydrolase in gad mice. *Nat. Genet.* **23**, 47–51.

Sambrook J. and Russell D. W. (2001) *Molecular Cloning: A Laboratory Manual*, 3rd edn. Cold Spring Harbor Laboratory Press, Cold Spring Harbor, NY.

Setsuie R., Wang Y. L., Mochizuki H. *et al.* (2007) Dopaminergic neuronal loss in transgenic mice expressing the Parkinson's disease-associated UCH-L1 I93M mutant. *Neurochem. Int.* **50**, 119–129.

Singleton A. B., Farrer M., Johnson J. *et al.* (2003) Alpha-synuclein locus triplication causes Parkinson's disease. *Science* **302**, 841.

Spillantini M. G., Schmidt M. L., Lee V. M., Trojanowski J. Q., Jakes R. and Goedert M. (1997) Alpha-synuclein in Lewy bodies. *Nature* **388**, 839–840.

Wilkinson K. D., Lee K. M., Deshpande S., Duerksen-Hughes P., Boss J. M. and Pohl J. (1989) The neuron-specific protein PGP 9.5 is a ubiquitin carboxyl-terminal hydrolase. *Science* **246**, 670–673.

Xu J., Kao S. Y., Lee F. J., Song W., Jin L. W. and Yankner B. A. (2002) Dopamine-dependent neurotoxicity of alpha-synuclein: a mechanism for selective neurodegeneration in Parkinson disease. *Nat. Med.* **8**, 600–606.

Yamada M., Iwatsubo T., Mizuno Y. and Mochizuki H. (2004) Overexpression of alpha-synuclein in rat substantia nigra results in loss of dopaminergic neurons, phosphorylation of alpha-synuclein and activation of caspase-9: resemblance to pathogenetic changes in Parkinson's disease. *J. Neurochem.* **91**, 451–461.

Yasuda T., Miyachi S., Kitagawa R. *et al.* (2007) Neuronal specificity of alpha-synuclein toxicity and effect of Parkin co-expression in primates. *Neuroscience* **144**, 743–753.

Zarranz J. J., Alegre J., Gomez-Esteban J. C. *et al.* (2004) The new mutation, E46K, of alpha-synuclein causes Parkinson and Lewy body dementia. *Ann. Neurol.* **55**, 164–173.

Zhou Y., Gu G., Goodlett D. R., Zhang T., Pan C., Montine T. J., Montine K. S., Aebersold R. H. and Zhang J. (2004) Analysis of alpha-synuclein-associated proteins by quantitative proteomics. *J. Biol. Chem.* **279**, 39155–39164.

Neurochemistry International xxx (2009) xxx–xxx

Contents lists available at ScienceDirect

Neurochemistry International

journal homepage: www.elsevier.com/locate/neuint

Proteomic and histochemical analysis of proteins involved in the dying-back-type of axonal degeneration in the gracile axonal dystrophy (*gad*) mouse

Akiko Goto [a,b], Yu-Lai Wang [a], Tomohiro Kabuta [a], Rieko Setsuie [a], Hitoshi Osaka [a], Akira Sawa [c], Shoichi Ishiura [b], Keiji Wada [a,*]

[a] Department of Degenerative Neurological Diseases, National Institute of Neuroscience, National Center of Neurology and Psychiatry, 4-1-1 Ogawahigashi, Kodaira, Tokyo, 187-8502, Japan
[b] Department of Life Sciences, Graduate School of Arts and Sciences, University of Tokyo, 3-8-1 Komaba, Meguro-ku, Tokyo,153-8902, Japan
[c] Depts. of Psychiatry and Neuroscience, Johns Hopkins University School of Medicine, Baltimore, MD 21287, USA

ARTICLE INFO

Article history:
Received 24 November 2008
Received in revised form 12 December 2008
Accepted 17 December 2008

Keywords:
Axonal degeneration
Dying-back
gad mouse
UCH-L1
Ubiquitin
2D-DIGE
GAPDH
Oxidative stress

ABSTRACT

Local axonal degeneration is a common pathological feature of peripheral neuropathies and neurodegenerative disorders of the central nervous system, including Alzheimer's disease, Parkinson's disease, and stroke; however, the underlying molecular mechanism is not known. Here, we analyzed the gracile axonal dystrophy (*gad*) mouse, which displays the dying-back-type of axonal degeneration in sensory neurons, to find the molecules involved in the mechanism of axonal degeneration. The *gad* mouse is analogous to a null mutant of ubiquitin carboxyl-terminal hydrolase L1 (UCH-L1). UCH-L1 is a deubiquitinating enzyme expressed at high levels in neurons, as well as testis and ovary. In addition, we recently discovered a new function of UCH-L1—namely to bind to and stabilize mono-ubiquitin in neurons, and found that the level of mono-ubiquitin was decreased in neurons, especially in axons of the sciatic nerve, in *gad* mice. The low level of ubiquitin suggests that the target proteins of the ubiquitin proteasome system are not sufficiently ubiquitinated and thus degraded in the *gad* mouse; therefore, these proteins may be the key molecules involved in axonal degeneration. To identify molecules involved in axonal degeneration in *gad* mice, we compared protein expression in sciatic nerves between *gad* and wild-type mice at 2 and 12 weeks old, using two-dimensional difference gel electrophoresis. As a result, we found age-dependent accumulation of several proteins, including glyceraldehyde-3-phosphate dehydrogenase (GAPDH) and 14-3-3, in *gad* mice compared with wild-type mice. Histochemical analyses demonstrated that GAPDH and 14-3-3 were localized throughout axons in both *gad* and wild-type mice, but GAPDH accumulated in the axons of *gad* mice. Recently, it has been suggested that a wide range of neurodegenerative diseases are characterized by the accumulation of intracellular and extracellular protein aggregates, and it has been reported that oxidative stress causes the aggregation of GAPDH. Furthermore, histochemical analysis demonstrated that sulfonated GAPDH, a sensor of oxidative stress that elicits cellular dysfunction, was expressed in the axons of *gad* mice, and 4-hydroxy-2-nonenal, a major marker of oxidative stress, was also only detected in *gad* mice. Our findings suggest that GAPDH may participate in a process of the dying-back-type of axonal degeneration in *gad* mice and may provide valuable insight into the mechanisms of axonal degeneration.

1. Introduction

Axonal degeneration occurs in several chronic neurodegenerative diseases and in injuries caused by, for example, toxic, ischemic, or traumatic insults. Recent findings suggest that axonal degeneration precedes, and sometimes causes, neuronal death in these neurodegenerative disorders (Li et al., 2001; Ferri et al., 2003; Fischer et al., 2004; Stokin et al., 2005; Fischer and Glass, 2007), but the underlying molecular mechanism is not known.

The gracile axonal dystrophy (*gad*) mutant mouse is characterized by sensory ataxia at an early stage, followed by motor ataxia at a later stage (Yamazaki et al., 1988; Saigoh et al., 1999). Pathologically, axonal degeneration in the *gad* mouse begins with the distal ends of primary ascending axons in the dorsal root ganglia (DRG) (Mukoyama et al., 1989; Kikuchi et al., 1990; Oda et al., 1992; Miura et al., 1993), and spheroid formation in the dying-back-type of axonal degeneration is observed in the gracile and dorsal spinocerebellar tracts (Yamazaki et al., 1988; Kikuchi

* Corresponding author. Tel.: +81 42 346 1715 fax: +81 42 346 1745.
E-mail address: wada@ncnp.go.jp (K. Wada).

0197-0186/$ – see front matter © 2008 Elsevier Ltd. All rights reserved.
doi:10.1016/j.neuint.2008.12.012

Please cite this article in press as: Goto, A., et al., Proteomic and histochemical analysis of proteins involved in the dying-back-type of axonal degeneration in the gracile axonal dystrophy (*gad*) mouse. Neurochem. Int. (2009), doi:10.1016/j.neuint.2008.12.012

et al., 1990; Miura et al., 1993). At a later stage, axonal degeneration and spheroid formation are observed at both the central and peripheral ends of DRG neurons and extend transsynaptically to the upper tracts as well as to motor neurons (Mukoyama et al., 1989; Kikuchi et al., 1990; Oda et al., 1992; Miura et al., 1993). Therefore, the *gad* mouse is an effective model for analyzing the molecular mechanism of the dying-back-type of axonal degeneration.

Previously, we found that the *gad* mutation is caused by an in-frame deletion of *Uchl1*, which encodes ubiquitin carboxyl-terminal hydrolase L1 (UCH-L1) (Saigoh et al., 1999). UCH-L1 is expressed at high levels in neurons, as well as testis and ovary, and constitutes ~5% of total soluble protein in the brain (Wilkinson et al., 1989). UCH-L1 is reported to be one of the deubiquitinating enzymes in the ubiquitin-proteasome system (UPS), where it hydrolyzes bonds between ubiquitin (Ub) and small adducts and creates free mono-Ub *in vitro* (Larsen et al., 1998). UCH-L1 also acts as a Ub ligase *in vitro* (Liu et al., 2002). In addition, we recently found a new function for UCH-L1—to bind to and stabilize mono-Ub in neurons (Osaka et al., 2003).

Using histochemical analysis, we previously demonstrated that UCH-L1 and mono-Ub are colocalized in axons of the sciatic nerve. In *gad* mice, the level of mono-Ub was decreased in neurons, especially in axons of the sciatic nerve (Osaka et al., 2003). The low level of ubiquitin suggests that the target proteins of the ubiquitin-proteasome system (UPS) are not sufficiently ubiquitinated and thus degraded in the *gad* mouse; therefore, these proteins may be key molecules involved in axonal degeneration. To identify the molecules involved in axonal degeneration in *gad* mice, we analyzed protein expression in sciatic nerves using two-dimensional difference gel electrophoresis (2D-DIGE).

Proteomic approaches compare protein expression comprehensively; 2D-DIGE is a modification of the traditional 2D technology, in which small amounts of multiple protein samples can be compared together, because each sample can be pre-labeled with different fluorescence dyes, mixed together, and run on the same isoelectric focusing (IEF) gel and SDS-PAGE (Knowles et al., 2003; Shaw and Riederer, 2003). We used 2D-DIGE because it is the most efficient method for analyzing the small amount of protein that can be extracted from a sciatic nerve. Here, we show that there are age-dependent accumulations of several proteins, including glyceraldehyde-3-phosphate dehydrogenase (GAPDH) and 14-3-3, in *gad* mice compared with wild-type (WT) mice, suggesting that these proteins are involved in axonal degeneration.

2. Experimental procedures

2.1. Animals

We used homozygous *gad* mice and their wild-type siblings (Harada et al., 2004; Wang et al., 2004). Mice were maintained and propagated at the National Institute of Neuroscience, National Center of Neurology and Psychiatry, Japan. Proteomic studies were carried out at 2 and 12 weeks old. Western blotting analyses were carried out at 12 weeks old. Histochemical analyses were carried out at 7 and 12 weeks old. Animals were anesthetized with Nembutal, and the sciatic nerve was perfused with saline. All mouse experiments were performed in accordance with our institution's regulations for animal care and with the approval of the Animal Investigation Committee of the National Institute of Neuroscience, National Center of Neurology and Psychiatry which conforms to the National Institute of Health guide for the care and use of laboratory animals.

2.2. Preparation of protein samples and labeling of protein samples with Cy dyes

Each sciatic nerve was suspended in 300 μl of sample buffer, containing 7 M urea, 2 M thiourea, 4% (w/v) CHAPS, and 40 mM Tris base (pH 8.0), by sonication for 60 s on ice, gently vortexed, and centrifuged for 20 min at 14,000 × *g* at 4 °C. Protein concentration was determined using a 2-D Quant Kit (GE Healthcare, Piscataway, NJ, USA). Protein samples were labeled as recommended by the manufacturer (GE Healthcare) using 400 pmol Cy dyes (GE Healthcare) per 50 μg of protein. Separate solutions containing 15 μg of protein from one *gad* or WT sample were labeled with Cy3 or Cy5 dye, respectively, and a common pool of proteins with *gad* and WT samples mixed equally were labeled with Cy2 dye by vortexing and incubating on ice in the dark for 30 min. The labeled samples were quenched by the addition of 1 μl 10 mM lysine (Sigma–Aldrich, St. Louis, MO, USA) and incubated on ice for 10 min.

2.3. Two-dimensional polyacrylamide gel electrophoresis (2D PAGE)

The quenched Cy3, Cy5, and Cy2 samples (15 μg of protein each) were mixed and denatured in 2D PAGE sample buffer containing 7 M urea, 2 M thiourea, 4% (w/v) CHAPS, 0.2% DTT, and 1.4% Ampholine. For the IEF, 45 μg of protein was applied to a rehydrated Immobiline Drystrip (pH 3–10, 7 cm; GE Healthcare) in a strip holder and incubated overnight in the dark. IEF was performed using a Multiphor II Electrophoresis system (GE Healthcare). The electrophoresis conditions were set as follows: step 1, 200 V for 1 min; step 2, 3500 V for 90 min; step 3, 3500 V for 125 min. After IEF, the strip was equilibrated with SDS buffer and applied to the 12.5% 2D SDS-PAGE for the analysis of 12-week-old mice and to the 4–20% SDS-PAGE for the analysis of 2-week-old mice using a precast Multigel II system (Daiichi Kagaku, Japan).

2.4. Image analysis and statistics

We scanned 2D gels using a Typhoon 9000 fluorescent imager (GE Healthcare). Excitation/emission wavelengths were chosen for each of the dyes. Gel images were preprocessed to remove extraneous areas using ImageQuant V5.0 (GE Healthcare). Gel analysis was performed using DeCyder DIA V5.0 (Difference In-gel Analysis; GE Healthcare). In-gel matching and statistical analysis were performed using DeCyder BVA V5.0 (Biological Variance Analysis; GE Healthcare). The Student's paired *t*-test ($P < 0.05$) was performed to identify the protein spots that were differentially expressed between *gad* and WT mice.

2.5. In-gel digestion and analysis by matrix-assisted laser desorption/ionization tandem time-of-flight (MALDI-TOF/TOF) mass spectrometry

To identify a particular protein in a spot detected by 2D-DIGE analysis, sciatic nerve extract containing 100 μg of protein was subjected to 12.5% 2D SDS-PAGE and stained with Coomassie brilliant blue (Invitrogen). The spots of interest were excised from the gel, destained, dehydrated with acetonitrile for 10 min, and completely dried under a vacuum pump for 10 min. Each spot was placed in 20 μl of 5 mM NH_4HCO_3 containing 1 pmol of sequencing-grade trypsin (Promega, Madison, WI, USA) overnight at 37 °C. Aliquots of the trypsinized samples were analyzed by nanoliquid chromatography and automatically spotted with alpha-cyano-4-hydroxy-cinnamic acid solution on a stainless-steel target and air dried. All mass spectra were obtained with MALDI-TOF/TOF (AXIMA-CFR; Shimadzu, Japan). MALDI peptide spectra were calibrated using several peaks of self-digested trypsin and matrix ion as internal standards.

2.6. Protein identification

Protein identification was performed using database searches on the web with Mascot Wizard (Matrix Science Ltd., London, United Kingdom). Criteria for protein identification were as follows: mascot score higher than 80 and mass tolerance of 100 ppm. Calculated pI and molecular mass data were obtained by Mascot.

2.7. 2D Western blotting for identification of GAPDH

One protein spot that was increased in *gad* mice but could not be detected by MALDI-TOF/TOF analysis was speculated to be GAPDH from its isoelectric point, molecular weight and location of the 2D gel compared with the mouse brain proteome database, and was therefore subjected to 2D Western blotting using an anti-GAPDH antibody (1:200, Chemicon, MAB374). One-hundred μg of sciatic nerve proteins were separated by 12.5% 2D SDS-PAGE and transferred onto a PVDF membrane (Immobilon-P; Millipore, Bedford, MA, USA). The membrane was washed with MilliQ water for 1 h at room temperature. Western blotting was performed as described in the following section.

2.8. Western blotting

Using 4–20% gradient SDS-PAGE, 2 μg of total protein was separated and transferred onto a PVDF membrane (Immobilon-P; Millipore). The membrane was washed with MilliQ water, then blocked with 5% skim milk in 0.05% Tween 20 in TBS (TTBS) for 1 h at room temperature, and incubated with primary antibodies in TTBS overnight at 4 °C. Primary antibodies used in this study were anti-UCH-L1 polyclonal antibody (1:5000, UltraClone, RA95101), anti-GAPDH monoclonal antibody (1:200, Chemicon, MAB374), anti-14-3-3 polyclonal antibody (1:100, IBL, 18649), anti-neurofilament L monoclonal antibody (NF-L, 1:500, Chemicon, MAB1615), anti-neuronal class III β tubulin antibody (βTUBIII, 1:1000, Covance, TUJ1), and anti-actin monoclonal antibody (1:4000, Sigma, AC-15). After washing, the membranes were incubated for 1 h at room temperature with either anti-mouse or anti-rabbit IgG horseradish peroxidase (HRP) conjugated secondary antibodies (1:10,000, GE Healthcare). Protein signals were detected with SuperSignal West Femto Maximum Sensitivity Substrate (Pierce) and were visualized with the LAS-3000 imaging system (Fujifilm, Tokyo, Japan).

Please cite this article in press as: Goto, A., et al., Proteomic and histochemical analysis of proteins involved in the dying-back-type of axonal degeneration in the gracile axonal dystrophy (*gad*) mouse. Neurochem. Int. (2009), doi:10.1016/j.neuint.2008.12.012

2.9. Immunohistochemistry

Mice were anesthetized and perfused with ice-cold 4% paraformaldehyde in phosphate-buffered saline (PBS, pH 7.4). Sciatic nerves were collected and postfixed in 4% paraformaldehyde overnight at 4 °C. The samples were embedded in paraffin and sectioned at 5 μm for immunohistochemistry. Serial sections were deparaffinized in xylene and graded ethanol, and washed in distilled water. Sections were blocked by incubation in 10% normal goat serum for 30 min at room temperature and incubated overnight at 4 °C with diluted primary antibodies. The following antibodies were used at the final dilutions indicated: anti-GAPDH polyclonal antibody (1:1000), anti-sulfonated GAPDH polyclonal antibody (1:500; these two antibodies were kindly provided by Dr. Sawa), anti-14-3-3 polyclonal antibody (1:100, IBL, 18649), anti-myelin basic protein monoclonal antibody (MBP, 1:200, QED Bioscience, 24201), anti-neurofilament M monoclonal antibody (NF-M, 1:200, Chemicon, MAB1621), anti-UCH-L1 polyclonal antibody (1:2000, UltraClone, RA95101), anti-UCH-L1 monoclonal antibody (1:200; Medac, Wedel, Germany), βTUBIII (1:300, COVANCE, TUJ1), and anti-4-hydroxy-2-nonenal monoclonal antibody (HNE, 25 μg/ml, JalCA, Shizuoka, Japan).

After incubating with primary antibodies, sections were washed 5 times with 0.1% Tween 20 in PBS (PBST) for 5 min at room temperature and then incubated for 90 min at room temperature with diluted secondary antibodies. The following antibodies were used at the final dilutions indicated: anti-mouse-Alexa594 IgG and anti-rabbit-Alexa588 IgG (1:400, Invitrogen) for immunofluorescence staining, or EnVision+ anti-rabbit HRP (Dako, Japan) for DAB staining. For DAB staining, bound antibody complexes were visualized using DAB (Dako, Japan) as a peroxidase substrate. Primary and secondary antibodies were diluted in Dako Antibody Diluent (Dako, Japan). After incubation with secondary antibodies, sections were washed 5 times with PBST for 5 min at room temperature and mounted with Antifade Kit (Molecular Probes). For analysis of 14-3-3 and HNE, sections were pretreated in a microwave oven for 10 min in citrate buffer solution (pH 6.0), cooled down, and washed 3 times for 5 min in PBS at room temperature. For the other immunostaining analyses, this pretreatment was not needed. For DAB staining, sections were treated with 3% H_2O_2 in methanol for 5 min to quench endogenous peroxidase activity before treatment with the primary antibodies.

3. Results

3.1. Analyses of differentially expressed proteins between gad and WT mice by 2D-DIGE

To find proteins that are upregulated in *gad* mice compared with WT mice, we analyzed sciatic nerves from 3 *gad* and 3 WT mice at 2 weeks old as well as at 12 weeks old, using 2D-DIGE technology. The proteins from *gad* mice were pre-labeled with Cy5 (red), and the proteins from WT mice were pre-labeled with Cy3 (green), respectively. A common pool of proteins composed of an equal amount of protein from a single *gad* and WT mouse was pre-labeled with Cy2, and the same manipulation was performed in 3 independent experiments.

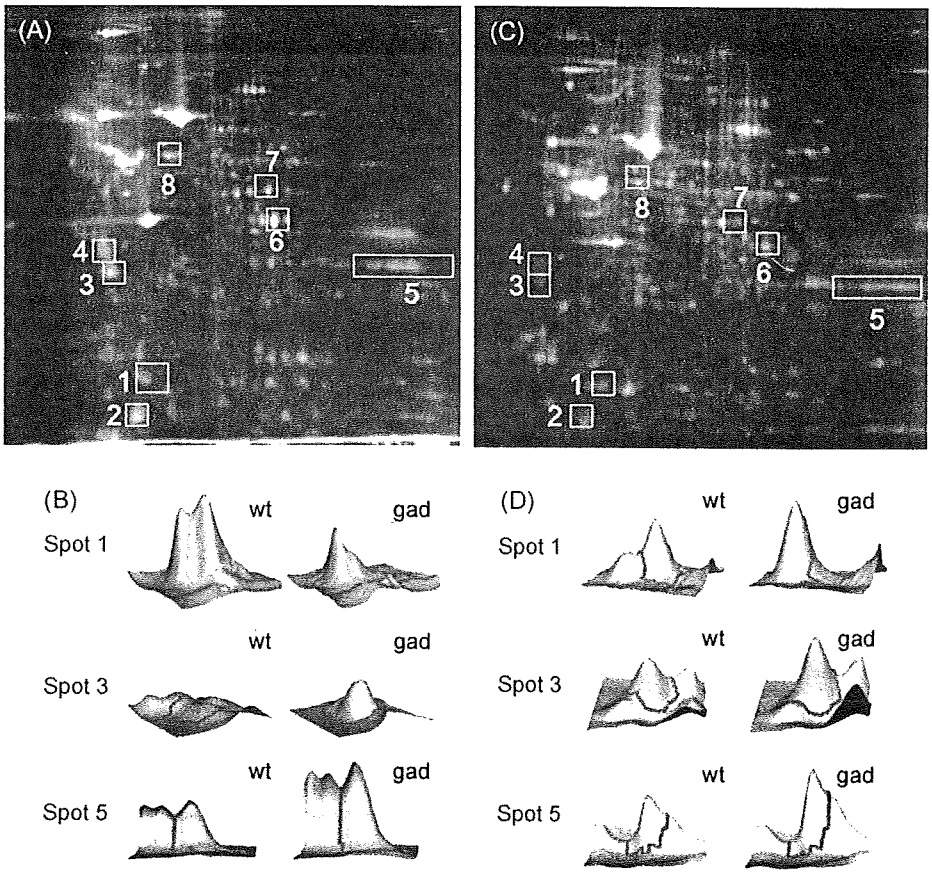

Fig. 1. Analyses of differentially expressed proteins between *gad* and wild-type mice by two-dimensional difference gel electrophoresis (2D-DIGE).
(A) A representative pseudocolor picture of superimposed DIGE images of mice at 12 weeks old. Fourteen protein spots are increased in *gad* mice compared with wild-type (WT) mice (red) by at least 1.6-fold (Student's paired *t*-test value; $P < 0.05$ in 3 parallel gels), and one spot is not detected at all in *gad* mice (green). Seven protein spots (spot No. 2–8) are increased in *gad* mice in an age-dependent manner, and one spot (spot No. 1) was not detected at all in *gad* mice at either 2 or 12 weeks old. The spot numbers of the latter differentiated 8 spots are shown in this map.
(B) A representative pseudocolor picture of superimposed DIGE images of mice at 2 weeks old. Eighteen protein spots are increased in *gad* mice compared with WT mice (red) by at least 1.6-fold (Student's paired *t*-test value; $P < 0.05$ in 3 parallel gels), and one spot is not detected at all in *gad* mice (green). The spot numbers in this figure are the same as in A.
(C) The 3D images of typical protein spots that were differentially expressed between *gad* and WT mice at 2 weeks old (spot numbers 1, 3, and 5 in A).
(D) The 3D images of typical protein spots that were differentially expressed between *gad* and WT mice at 2 weeks old (spot numbers 1, 3, and 5 in C) (For interpretation of the references to color in this figure legend, the reader is referred to the web version of the article.)

Please cite this article in press as: Goto, A., et al., Proteomic and histochemical analysis of proteins involved in the dying-back-type of axonal degeneration in the gracile axonal dystrophy (*gad*) mouse. Neurochem. Int. (2009), doi:10.1016/j.neuint.2008.12.012

Table 1
List of proteins differentially expressed between *gad* and WT mice.

Spot no.	Protein name	Score	Molecular mass (kDa)/pI	Av. ratio (*gad*/wt) 12 weeks	*P* value	Av. ratio (*gad*/wt) 2 weeks	*P* value
1	Ubiquitin thiolesterase PGP9.5 (UCH-L1)	96	25.10/5.12	−14.38	0.005	−3.89	0.003
3	14-3-3 protein	94	28.10/4.63	5.4	0.030	7.32	0.001
4	Annexin A5	143	35.79/4.83	6.68	0.020	5.19	0.030
8	Neurofilament triplet L protein (NF-L)	212	61.40/4.62	2.18	0.010	3.53	0.026
5	Glyceraldehyde 3-phosphate dehydrogenase (GAPDH)		38.07/8.34	3.89	0.043	1.61	

*GAPDH was detected by 2D Western blotting and not by MALDI-TOF/TOF.

Fig. 1A shows a representative pseudocolor picture of superimposed DIGE images of the 12-week-old mouse samples. Fourteen protein spots were increased by at least 1.6-fold in *gad* mice compared with WT mice (red; Student's paired *t*-test value; $P < 0.05$ in 3 parallel gels), and one spot was not detected at all in *gad* mice (green).

Fig. 1B shows a representative pseudocolor picture of superimposed DIGE images of the 2-week-old mouse samples. Eighteen protein spots were increased by at least 1.6-fold in *gad* mice compared with WT mice (red; Student's paired *t*-test value; $P < 0.05$ in 3 parallel gels), and one spot was not detected at all in *gad* mice (green).

Based on comparison of the 2D-DIGE analysis of mice between 2 and 12 weeks old, 7 protein spots showed an age-dependent increase in *gad* mice (spots No. 2–8). One spot (spot No. 1) was not detected at all in *gad* mice at either 2 or 12 weeks old (Fig. 1A and B).

Fig. 1C shows the 3D images of typical spots (spots No. 1, 3, and 5) in Fig. 1A, and Fig. 1D shows the 3D images of typical spots (spots No. 1, 3, and 5) in Fig. 1B.

3.2. Identification of differentially expressed proteins between gad and WT mice by MALDI-TOF/TOF and 2D Western blotting

The proteins of spots that were age dependently increased or absent in *gad* mice were analyzed by MALDI-TOF/TOF and identified (spots No. 1, 3, 4, and 8). The proteins were identified as UCH-L1 (spot No. 1), 14-3-3 (spot No. 3), annexin V (spot No. 4), and Neurofilament L (NF-L) (spot No. 8). Additionally, we speculated that spot No. 5 may represent GAPDH based on the information from the mouse brain proteome database (http://www.charite.de/humangenetik/klose_public1/index.html), and confirmed this by 2D Western blotting with GAPDH antibodies. The results of the protein identification are listed in Table 1, including spot number, protein name, mascot score, theoretical relative molecular mass, isoelectric point, average ratio of *gad*/wt protein level, and *P*-value using DeCyder, at both 2 and 12 weeks old.

3.3. Analyses of the expression levels of proteins in gad and WT mice by Western blotting

In 2D-DIGE system, each sample was pre-labeled with different fluorescence dyes, Cy3, Cy5 or Cy2. This labeling-process allows comparison of multiple samples in same 2D-gel, but it is reported that efficiency of each dyes to label proteins was not exactly the same. We assume that 2D-DIGE is reliable method to detect molecules involved in axonal degeneration but Western blot analysis using specific antibodies is more accurate, and in fact, it is usual that identified proteins by TOF-MASS are reconfirmed by Western blotting. Therefore, the expression levels of the proteins in

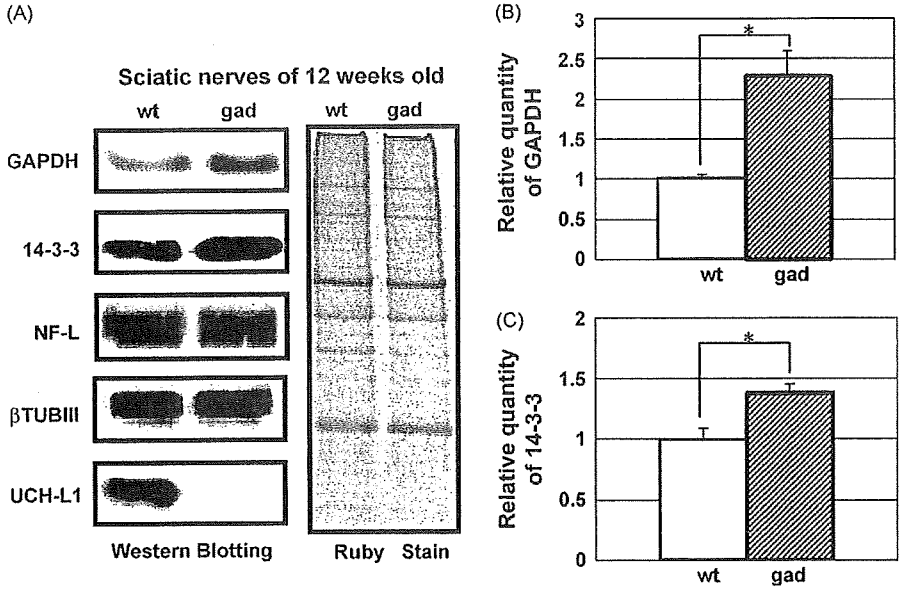

Fig. 2. Western blotting analyses of the expression levels of proteins expressed differentially between *gad* and WT mice.
(A) Results of Western blotting analysis with antibodies against ubiquitin carboxyl-terminal hydrolase L1 (UCH-L1), neurofilament L (NF-L), 14-3-3, glyceraldehyde-3-phosphate dehydrogenase (GAPDH), and classIII β tubulin (βTUBIII). GAPDH and 14-3-3 protein levels were increased in *gad* mice compared with WT mice.
(B) Quantification of the band intensities of GAPDH. Values are means ± SEM of 3 independent experiments (*$P < 0.05$); GAPDH is increased by about 2.3-fold in *gad* mice at 12 weeks old compared with WT mice.
(C) Quantification of the band intensities of 14-3-3. Values are means ± SEM of 3 independent experiments (*$P < 0.05$); 14-3-3 is increased by 1.3-fold in *gad* mice at 12 weeks old compared with WT mice.

Please cite this article in press as: Goto, A., et al., Proteomic and histochemical analysis of proteins involved in the dying-back-type of axonal degeneration in the gracile axonal dystrophy (*gad*) mouse. Neurochem. Int. (2009), doi:10.1016/j.neuint.2008.12.012

gad and WT mice listed in Table 1 were further analyzed by Western blotting to reconfirm the results of 2D-DIGE (Fig. 2A). We chose these proteins because they were all reported to be expressed in neurons. In 12-week-old *gad* mice, GAPDH was increased by an average ratio of 2.3-fold (Fig. 2B), and 14-3-3 was increased by an average ratio of 1.3-fold (Fig. 2C) compared with WT mice. The levels of NF-L and βTUBIII, which was used as an internal control, showed no significant difference between *gad* and WT mice at 12 weeks old (Fig. 2A). Annexin V was not analyzed because its antibodies did not work in this experimental system containing urea and thiourea. The same results were obtained in 3 independent experiments.

3.4. Histochemical localization of GAPDH in the sciatic nerves of gad and WT mice

Sciatic nerves are composed internally of neuronal axons and externally of myelin derived from glial Schwann cells, and protein samples in the proteomic analysis were a mixture of axons and myelin. We examined the histological localization of GAPDH, which was dominantly increased in *gad* mice, by double immunofluorescence staining using an antibody against GAPDH and the neuronal markers neurofilament M (NF-M) or UCH-L1, or the Schwann cells marker myelin basic protein (MBP). In *gad* mice, GAPDH was colocalized with MBP (Fig. 3A, right panel) but was more dominantly colocalized with NF-M, a neuronal marker (Fig. 3A, left panel). These results suggest that GAPDH is mainly localized in axons in *gad* mice. In WT mice, GAPDH was colocalized with the neuronal marker UCH-L1 (Fig. 3B, left panel). Because UCH-L1 is the product of the gene defective in the *gad* mouse, UCH-L1 is not detected in *gad* mice (Fig. 3B, right panel). The same results were obtained in 3 independent experiments.

3.5. DAB staining analyses of GAPDH and 14-3-3 in the sciatic nerves of gad and WT mice

We examined in detail the localization of GAPDH in cross or vertical sections of sciatic nerve axons by DAB staining (Figs. 4A–F). In the cross-sections, GAPDH was localized in axons in both *gad* and WT mice and was remarkably accumulated in *gad* mice compared with WT mice (Fig. 4A and B). In vertical sections, GAPDH was also localized in axons in both *gad* and WT mice (Fig. 4C–F). Notably, aggregates of GAPDH were observed in *gad* mice but not in WT mice (Fig. 4E and F, arrow). Next, we examined the expression of 14-3-3, which was found to be increased in *gad* mice upon 2D-DIGE and Western blotting analyses. In both *gad* and WT mice, 14-3-3 was expressed in axons, and there was no significant difference between *gad* and WT mice (Fig. 4G–J). The same results were obtained in 3 independent experiments.

3.6. Histochemical analyses of sulfonated GAPDH in the sciatic nerves of gad and WT mice

It was reported that oxidative stress induces the oligomerization and aggregation of GAPDH (Cumming and Schubert, 2005; Nakajima et al., 2007), and in this study we found that GAPDH is accumulated in axons of *gad* mice that exhibit a dying-back-type of axonal degeneration. Thus, we postulated that oxidative stress would be increased in *gad* mice, and therefore examined the expression of sulfonated GAPDH (Hara et al., 2005), in the sciatic

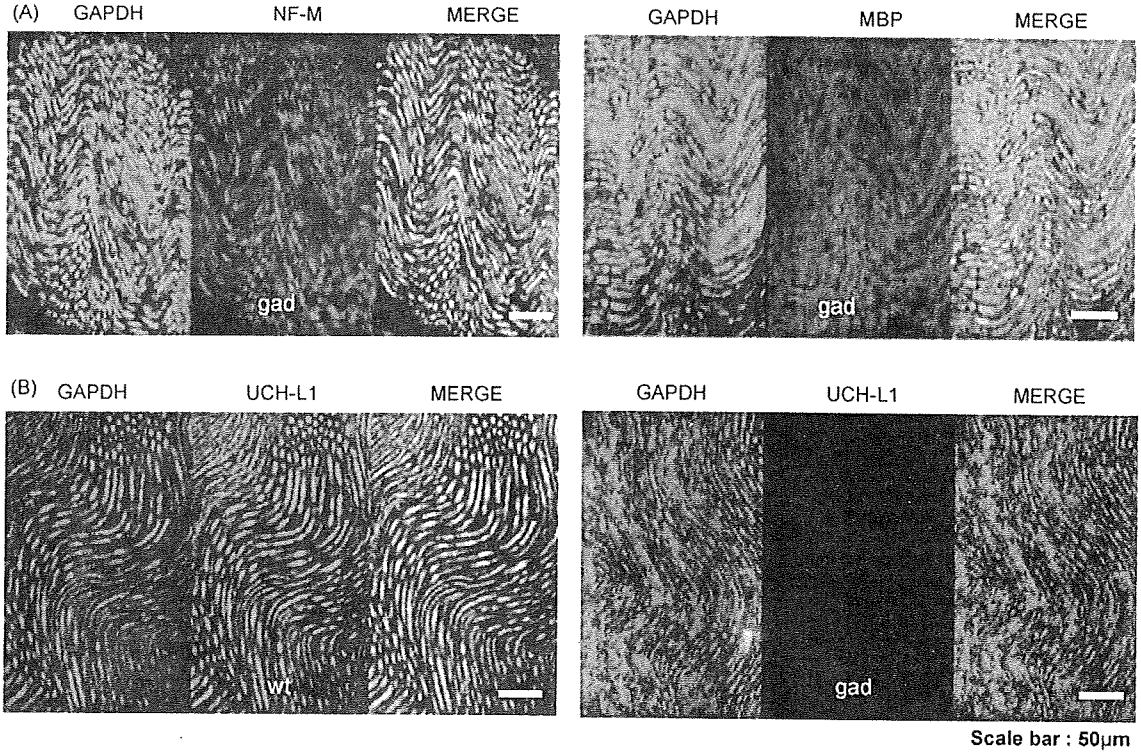

Fig. 3. Histochemical localization of GAPDH in the sciatic nerves of *gad* and WT mice.
(A) Double immunofluorescent staining of the sciatic nerve of *gad* mice using antibodies against GAPDH, neurofilament M (NF-M), or myelin basic protein (MBP). GAPDH was colocalized with NF-M (left panel) and partly with MBP (right panel) in *gad* mice. GAPDH is mainly localized in axons.
(B) Double immunofluorescent staining of the sciatic nerve of *gad* and WT mice using antibodies against GAPDH and UCH-L1. In WT mice, GAPDH is colocalized with UCH-L1 (left panel). In *gad* mice, UCH-L1 is not detected (right panel), and GAPDH is strongly detected compared with WT mice.

Please cite this article in press as: Goto, A., et al., Proteomic and histochemical analysis of proteins involved in the dying-back-type of axonal degeneration in the gracile axonal dystrophy (*gad*) mouse. Neurochem. Int. (2009), doi:10.1016/j.neuint.2008.12.012

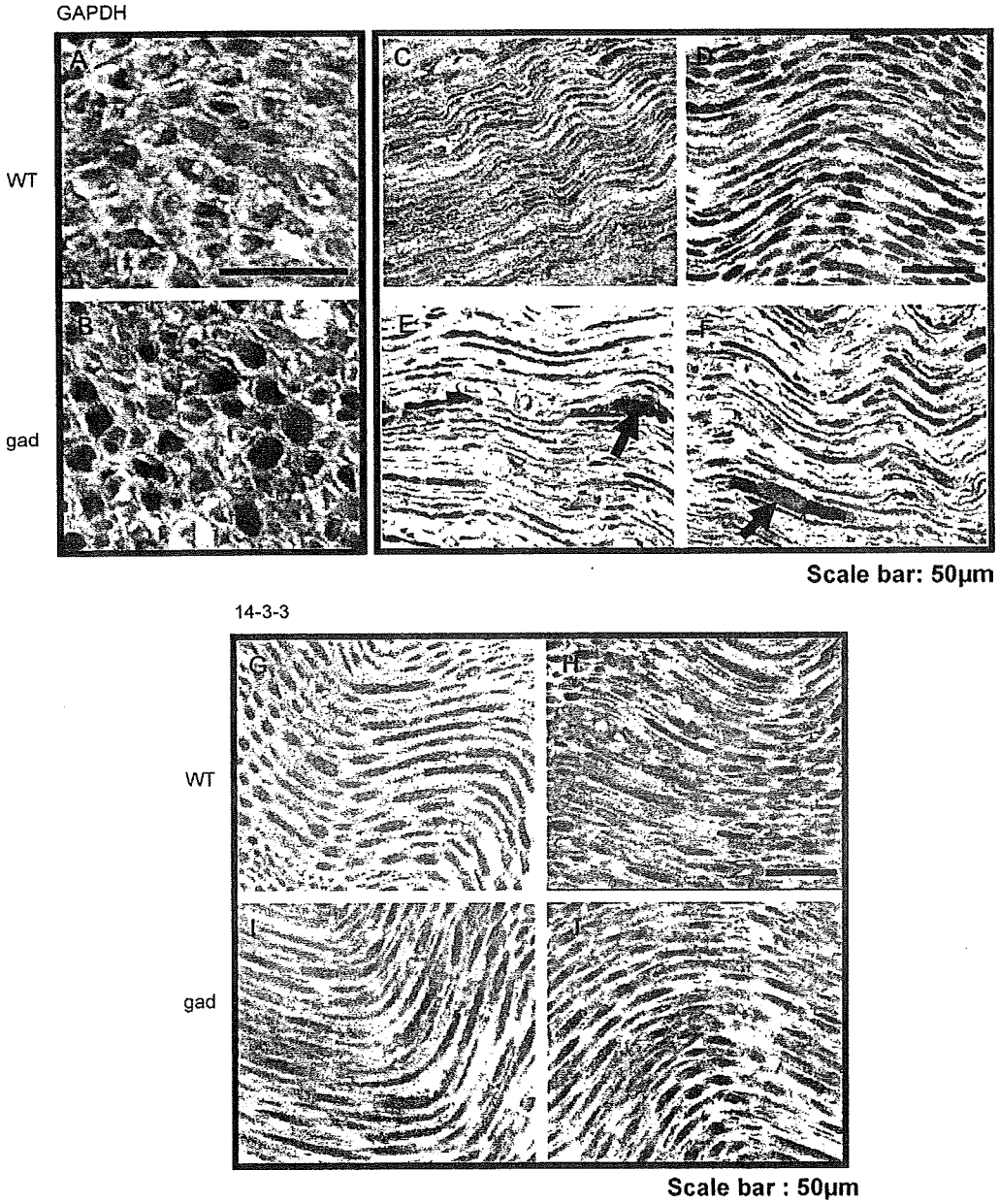

Fig. 4. DAB staining of GAPDH and 14-3-3 in the sciatic nerves of *gad* and WT mice.
(A–F) Sections of sciatic nerves of WT (A, C, and D) or *gad* (B, E, and F) mice stained with DAB using GAPDH antibodies.
(A) Cross-section of a sciatic nerve of a WT mouse. GAPDH is mainly localized in axons.
(B) Cross-section of a sciatic nerve of a *gad* mouse. GAPDH is mainly localized in axons and is highly expressed compared with the WT mouse.
(C and D) Vertical sections of sciatic nerves of WT mice. GAPDH is localized in axons.
(E and F) Vertical sections of sciatic nerves of *gad* mice. GAPDH is localized in axons and is accumulated. GAPDH aggregates are indicated by arrows.
(G–J) Sections of sciatic nerves of WT (G, H) and *gad* (I, J) mice stained with DAB using 14-3-3 antibodies.
(G and H) Vertical sections of sciatic nerves of WT mice; 14-3-3 is localized in axons of WT mice.
(I and J) Vertical sections of sciatic nerves of *gad* mice; 14-3-3 is localized in axons of *gad* mice, and there was no significant difference between *gad* and WT mice (G, H).

nerves of *gad* and WT mice. We found that although sulfonated GAPDH was not detected in WT mice, it was clearly detected in *gad* mice (Fig. 5A and B). In *gad* mice, sulfonated GAPDH was colocalized with the neuronal markers βTUBIII (Fig. 5B) and NF-M (data not shown) in axons. In *gad* mice, accumulated sulfonated GAPDH was also detected in the outer portion of the axons, around the DAPI staining for nuclei (Fig. 5C). Axons do not contain nuclei, so these DAPI signals may come from Schwann cells. The same results were obtained in 3 independent experiments.

3.7. *Histological analyses of HNE, a marker of oxidative stress, in the sciatic nerves of gad and WT mice*

The results shown in Fig. 5 suggest that the level of oxidative stress is increased in *gad* mice. Accordingly, we examined the existence of HNE, a major marker of oxidative stress, in addition to sulfonated GAPDH. HNE was detected in *gad* mice, but not in WT mice (Fig. 6). The same results were obtained in 3 independent experiments.

Please cite this article in press as: Goto, A., et al., Proteomic and histochemical analysis of proteins involved in the dying-back-type of axonal degeneration in the gracile axonal dystrophy (*gad*) mouse. Neurochem. Int. (2009), doi:10.1016/j.neuint.2008.12.012

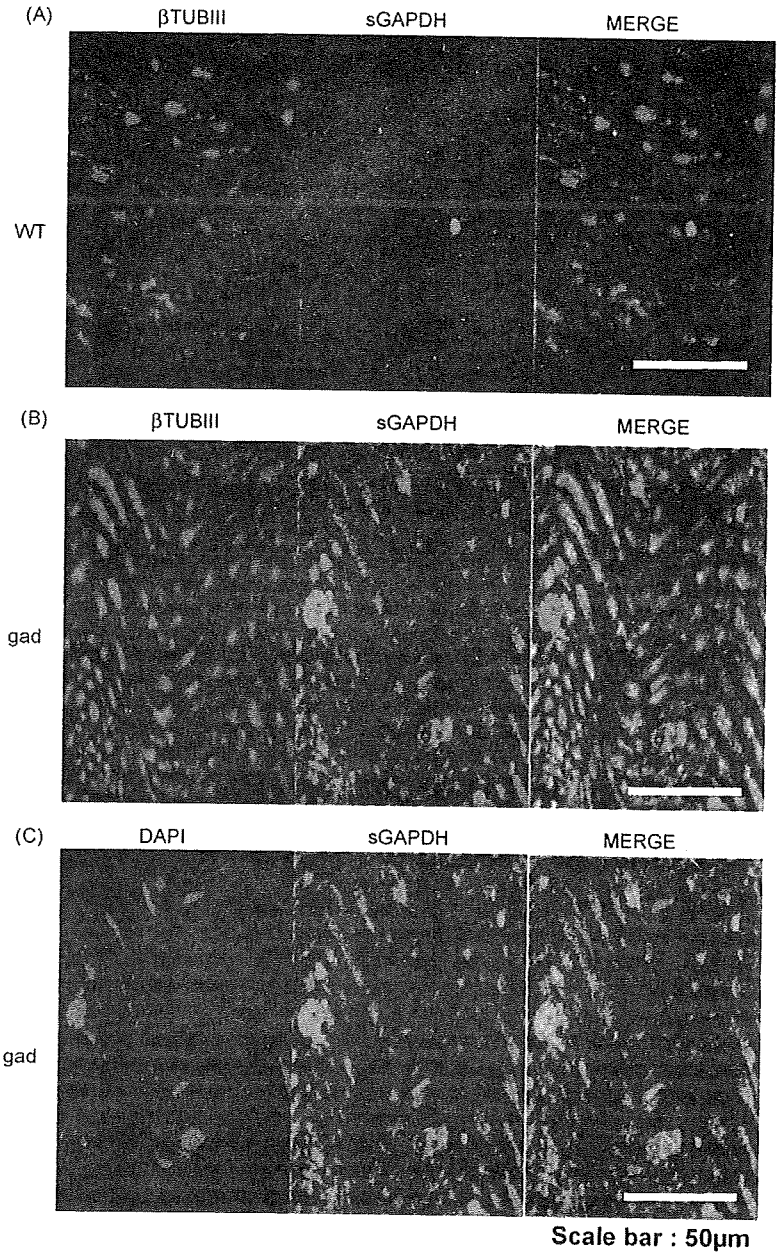

Fig. 5. Expression of sulfonated GAPDH in the sciatic nerves of *gad* and WT mice.
(A) Double immunofluorescent staining of a sciatic nerve of a WT mouse using antibodies against sulfonated GAPDH and βTUBIII. Sulfonated GAPDH was not detected in WT mice (middle panel).
(B) Double immunofluorescent staining of a sciatic nerve of a *gad* mouse using antibodies against sulfonated GAPDH and βTUBIII. In *gad* mice, sulfonated GAPDH was detected in axons of sciatic nerves (middle panel). Sulfonated GAPDH was colocalized with the neuronal marker βTUBIII in *gad* mice (right panel), as well as NF-M (data not shown). A representative result from 3 independent experiments is shown.
(C) Double immunofluorescent staining of a sciatic nerve of the *gad* mouse using an antibody against sulfonated GAPDH and DAPI. Sulfonated GAPDH was detected uniformaly within the axons of *gad* mice, and accumulation of sulfonated GAPDH was detected around the DAPI signals (right panel).

4. Discussion

In this study, we found that 14-3-3, annexin V, NF-L, and GAPDH were increased in an age-dependent manner in *gad* mice that display the dying-back-type of axonal degeneration, using 2D-DIGE analyses (Fig. 1). Based on Western blotting analyses, 14-3-3 and GAPDH were increased in *gad* mice compared with WT mice (Fig. 2). Histochemical analysis revealed that GAPDH was localized throughout axons and was accumulated in axons in *gad* mice compared with WT mice (Figs. 3 and 4). Also 14-3-3 was localized throughout axons, but there was no significant difference between *gad* and WT mice upon histochemical analyses, although it was increased in *gad* mice upon Western blotting analyses (Fig. 4). Since Western blotting showed only a slight increase in 14-3-3 (Fig. 2), we assume that this small difference could not be detected by histochemical analyses.

GAPDH is a classic glycolytic enzyme (Sirover, 1999; Chuang et al., 2005), and recent studies show that it is multifunctional

Please cite this article in press as: Goto, A., et al., Proteomic and histochemical analysis of proteins involved in the dying-back-type of axonal degeneration in the gracile axonal dystrophy (*gad*) mouse. Neurochem. Int. (2009), doi:10.1016/j.neuint.2008.12.012

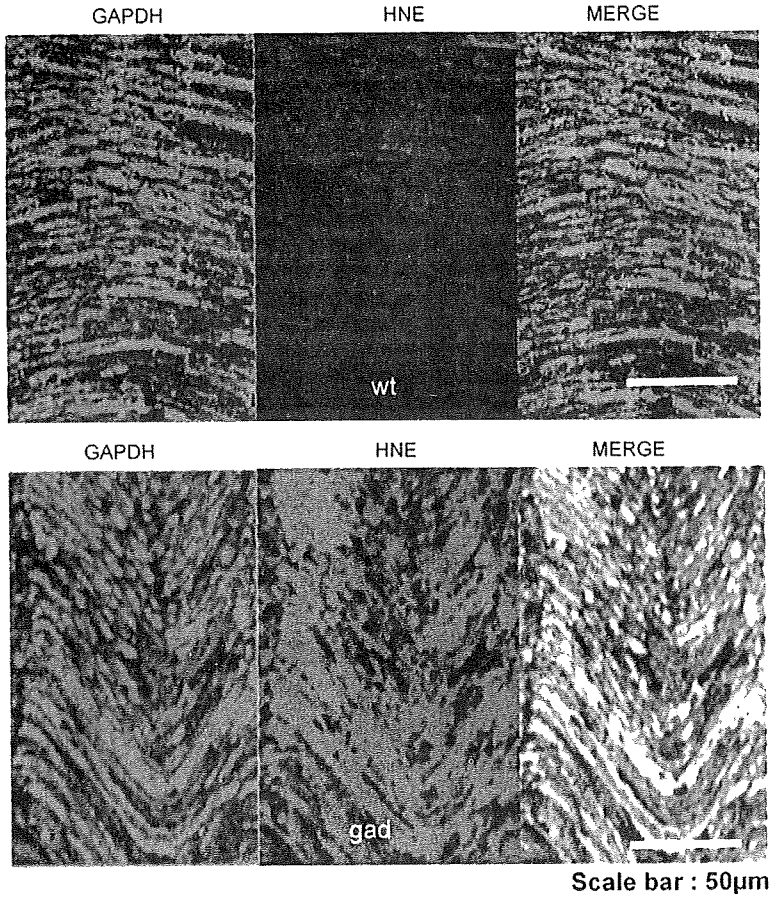

Fig. 6. Expression of HNE, a marker of oxidative stress, in the sciatic nerves of *gad* and WT mice.
Double immunofluorescent staining of sciatic nerves of *gad* and WT mice using antibodies against GAPDH and HNE. In WT mice, HNE was not detected (upper panel). On the other hand, HNE was strongly detected and mainly colocalized with GAPDH in *gad* mice (lower panel).

(Hara et al., 2006a). GAPDH has been reported to play roles in membrane fusion, microtubule bundling, nuclear RNA transport (Sirover, 1999), and transcription (Zheng et al., 2003). Particularly, its role as a mediator for cellular dysfunction/death has been highlighted (Sawa et al., 1997; Ishitani et al., 1998; Hara et al., 2005, 2006b). Sulfonation of GAPDH is reported to be induced by oxidative stress, and sulfonated GAPDH leads to cellular dysfunction (Hara et al., 2005, 2006a; Sen et al., 2008). Additionally, oxidative stress induces the oligomerization and aggregation of GAPDH through aberrant disulfide bonding of active-site cysteines, which leads to the formation of insoluble aggregates *in vitro* (Cumming and Schubert, 2005; Nakajima et al., 2007). Thus, GAPDH appears to participate in the mechanism leading to cellular dysfunction/death induced by oxidative stress. However, its function in axons or its association with axonal degeneration has not yet been demonstrated.

In this study, we found that GAPDH and sulfonated GAPDH were accumulated in *gad* mice compared with WT mice, suggesting that oxidative stress is increased in *gad* mice. In fact, we found that the oxidative stress marker HNE is increased in *gad* mice. It has also been reported that, the levels of carbonyl modification of proteins that is caused by oxidative stress are increased in the brains of *gad* mice compared with WT mice (Castegna et al., 2004). Therefore, we assume that accumulation of GAPDH and sulfonated GAPDH in the axons of *gad* mice were induced by oxidative stress.

Various molecules are involved in reduction-oxidative reactions, and recently the necessity of the UPS in reduction-oxidative reactions has been highlighted (Okada et al., 1999; Kang et al., 2008). It has been reported that a number of oxidative stress sensors are regulated by the UPS (Iwai, 2003; Kobayashi et al., 2004; Hara et al., 2006a). In *gad* mice, free-Ub pools are decreased in neurons, and proteolysis in the UPS is thought to be abnormal (Osaka et al., 2003). Oxidative stress is therefore expected to be increased in *gad* mice, which is consistent with our findings.

There is another possible mechanism for the accumulation of GAPDH in the axons of *gad* mice. GAPDH is reported to be degraded mainly by chaperone-mediated autophagy (Aniento et al., 1993; Cuervo et al., 1997). Our recent study showed that UCH-L1 physically interacts with lysosome-associated membrane protein type 2A, which is a component of CMA (Kabuta et al., 2008); thus CMA is possibly altered in the neuronal system of *gad* mice, potentially leading to the accumulation of GAPDH in the axons of *gad* mice.

This study demonstrates the alteration of GAPDH in axons of the *gad* mouse, a mutant with a loss of function of UCH-L1. Our findings suggest that GAPDH may participate in the process leading to the dying-back-type of axonal degeneration in *gad* mice and may provide valuable insight into the mechanisms of axonal degeneration.

Please cite this article in press as: Goto, A., et al., Proteomic and histochemical analysis of proteins involved in the dying-back-type of axonal degeneration in the gracile axonal dystrophy (*gad*) mouse. Neurochem. Int. (2009), doi:10.1016/j.neuint.2008.12.012

Acknowledgements

We thank the following people for their contributions to this work: Dr. Hidemitsu Nakajima (Osaka Prefecture University), Dr. Satoshi Nagamine (National Center of Neurology and Psychiatry) and Dr. Makoto R. Hara (Johns Hopkins University School of Medicine) for helpful discussions; Ms. Hisae Kikuchi (National Center of Neurology and Psychiatry) for technical assistance with tissue sections; Ms. Masako Shikama (National Center of Neurology and Psychiatry) for the care and breeding of animals; Dr. Hayato Onishi (University of Tokyo) for assistance with the TOF MASS analysis; and Dr. H. Akiko Popiel (National Center of Neurology and Psychiatry) for support with English; Mitsubishi Tanabe Pharma Corporation for giving a chance to A.G. of admission to doctoral course. This work was supported in part by Grants-in-Aid for Scientific Research from the Ministry of Health, Labour and Welfare of Japan, Grants-in-Aid for Scientific Research from the Ministry of Education, Culture, Sports, Science and Technology of Japan, the Program for Promotion of Fundamental Studies in Health Sciences of the National Institute of Biomedical Innovation, and a grant from Japan Science and Technology Agency.

References

Aniento, F., Roche, E., Cuervo, A.M., Knecht, E., 1993. Uptake and degradation of glyceraldehyde-3-phosphate dehydrogenase by rat liver lysosomes. J. Biol. Chem. 268, 10463–10470.

Castegna, A., Thongboonkerd, V., Klein, J., Lynn, B.C., Wang, Y.L., Osaka, H., Wada, K., Butterfield, D.A., 2004. Proteomic analysis of brain proteins in the gracile axonal dystrophy (gad) mouse, a syndrome that emanates from dysfunctional ubiquitin carboxyl-terminal hydrolase L-1, reveals oxidation of key proteins. J. Neurochem. 88, 1540–1546.

Chuang, D.M., Hough, C., Senatorov, V.V., 2005. Glyceraldehyde-3-phosphate dehydrogenase, apoptosis, and neurodegenerative diseases. Annu. Rev. Pharmacol. Toxicol. 45, 269–290.

Cuervo, A.M., Dice, J.F., Knecht, E., 1997. A population of rat liver lysosomes responsible for the selective uptake and degradation of cytosolic proteins. J. Biol. Chem. 272, 5606–5615.

Cumming, R.C., Schubert, D., 2005. Amyloid-beta induces disulfide bonding and aggregation of GAPDH in Alzheimer's disease. FASEB J. 19, 2060–2062.

Ferri, A., Sanes, J.R., Coleman, M.P., Cunningham, J.M., Kato, A.C., 2003. Inhibiting axon degeneration and synapse loss attenuates apoptosis and disease progression in a mouse model of motoneuron disease. Curr. Biol. 13, 669–673.

Fischer, L.R., Culver, D.G., Tennant, P., Davis, A.A., Wang, M., Castellano-Sanchez, A., Khan, J., Polak, M.A., Glass, J.D., 2004. Amyotrophic lateral sclerosis is a distal axonopathy: evidence in mice and man. Exp. Neurol. 185, 232–240.

Fischer, L.R., Glass, J.D., 2007. Axonal degeneration in motor neuron disease. Neurodegener. Dis. 4, 431–442.

Hara, M.R., Agrawal, N., Kim, S.F., Cascio, M.B., Fujimuro, M., Ozeki, Y., Takahashi, M., Cheah, J.H., Tankou, S.K., Hester, L.D., Ferris, C.D., Hayward, S.D., Snyder, S.H., Sawa, A., 2005. S-nitrosylated GAPDH initiates apoptotic cell death by nuclear translocation following Siah1 binding. Nat. Cell. Biol. 7, 665–674.

Hara, M.R., Cascio, M.B., Sawa, A., 2006a. GAPDH as a sensor of NO stress. Biochim. Biophys. Acta 1762, 502–509.

Hara, M.R., Thomas, B., Cascio, M.B., Bae, B.I., Hester, L.D., Dawson, V.L., Dawson, T.M., Sawa, A., Snyder, S.H., 2006b. Neuroprotection by pharmacologic blockade of the GAPDH death cascade. Proc. Natl. Acad. Sci. U.S.A. 103, 3887–3889.

Harada, T., Harada, C., Wang, Y.L., Osaka, H., Amanai, K., Tanaka, K., Takizawa, S., Setsuie, R., Sakurai, M., Sato, Y., Noda, M., Wada, K., 2004. Role of ubiquitin carboxy terminal hydrolase-L1 in neural cell apoptosis induced by ischemic retinal injury in vivo. Am. J. Pathol. 164, 59–64.

Ishitani, R., Tanaka, M., Sunaga, K., Katsube, N., Chuang, D.M., 1998. Nuclear localization of overexpressed glyceraldehyde-3-phosphate dehydrogenase in cultured cerebellar neurons undergoing apoptosis. Mol. Pharmacol. 53, 701–707.

Iwai, K., 2003. An ubiquitin ligase recognizing a protein oxidized by iron: implications for the turnover of oxidatively damaged proteins. J. Biochem. 134, 175–182.

Kabuta, T., Furuta, A., Aoki, S., Furuta, K., Wada, K., 2008. Aberrant interaction between Parkinson disease-associated mutant UCH-L1 and the lysosomal receptor for chaperone-mediated autophagy. J. Biol. Chem. 283, 23731–23738.

Kang, S.I., Choi, H.W., Kim, I.Y., 2008. Redox-mediated modification of PLZF by SUMO-1 and ubiquitin. Biochem. Biophys. Res. Commun. 369, 1209–1214.

Kikuchi, T., Mukoyama, M., Yamazaki, K., Moriya, H., 1990. Axonal degeneration of ascending sensory neurons in gracile axonal dystrophy mutant mouse. Acta Neuropathol. 80, 145–151.

Knowles, M.R., Cervino, S., Skynner, H.A., Hunt, S.P., de Felipe, C., Salim, K., Meneses-Lorente, G., McAllister, G., Guest, P.C., 2003. Multiplex proteomic analysis by two-dimensional differential in-gel electrophoresis. Proteomics 3, 1162–1171.

Kobayashi, A., Kang, M.I., Okawa, H., Ohtsuji, M., Zenke, Y., Chiba, T., Igarashi, K., Yamamoto, M., 2004. Oxidative stress sensor Keap1 functions as an adaptor for Cul3-based E3 ligase to regulate proteasomal degradation of Nrf2. Mol. Cell. Biol. 24, 7130–7139.

Larsen, C.N., Krantz, B.A., Wilkinson, K.D., 1998. Substrate specificity of deubiquitinating enzymes: ubiquitin C-terminal hydrolases. Biochemistry 37, 3358–3368.

Li, H., Li, S.H., Yu, Z.X., Shelbourne, P., Li, X.J., 2001. Huntingtin aggregate-associated axonal degeneration is an early pathological event in Huntington's disease mice. J. Neurosci. 21, 8473–8481.

Liu, Y., Fallon, L., Lashuel, H.A., Liu, Z., Lansbury Jr., P.T., 2002. The UCH-L1 gene encodes two opposing enzymatic activities that affect alpha-synuclein degradation and Parkinson's disease susceptibility. Cell 111, 209–218.

Miura, H., Oda, K., Endo, C., Yamazaki, K., Shibasaki, H., Kikuchi, T., 1993. Progressive degeneration of motor nerve terminals in GAD mutant mouse with hereditary sensory axonopathy. Neuropathol. Appl. Neurobiol. 19, 41–51.

Mukoyama, M., Yamazaki, K., Kikuchi, T., Tomita, T., 1989. Neuropathology of gracile axonal dystrophy (GAD) mouse. An animal model of central distal axonopathy in primary sensory neurons. Acta Neuropathol. 79, 294–299.

Nakajima, H., Amano, W., Fujita, A., Fukuhara, A., Azuma, Y.T., Hata, F., Inui, T., Takeuchi, T., 2007. The active site cysteine of the proapoptotic protein glyceraldehyde-3-phosphate dehydrogenase is essential in oxidative stress-induced aggregation and cell death. J. Biol. Chem. 282, 26562–26574.

Oda, K., Yamazaki, K., Miura, H., Shibasaki, H., Kikuchi, T., 1992. Dying back type axonal degeneration of sensory nerve terminals in muscle spindles of the gracile axonal dystrophy (GAD) mutant mouse. Neuropathol. Appl. Neurobiol. 18, 265–281.

Okada, K., Wangpoengtrakul, C., Osawa, T., Toyokuni, S., Tanaka, K., Uchida, K., 1999. 4-Hydroxy-2-nonenal-mediated impairment of intracellular proteolysis during oxidative stress. Identification of proteasomes as target molecules. J. Biol. Chem. 274, 23787–23793.

Osaka, H., Wang, Y.L., Takada, K., Takizawa, S., Setsuie, R., Li, H., Sato, Y., Nishikawa, K., Sun, Y.J., Sakurai, M., Harada, T., Hara, Y., Kimura, I., Chiba, S., Namikawa, K., Kiyama, H., Noda, M., Aoki, S., Wada, K., 2003. Ubiquitin carboxy-terminal hydrolase L1 binds to and stabilizes monoubiquitin in neuron. Hum. Mol. Genet. 12, 1945–1958.

Saigoh, K., Wang, Y.L., Suh, J.G., Yamanishi, T., Sakai, Y., Kiyosawa, H., Harada, T., Ichihara, N., Wakana, S., Kikuchi, T., Wada, K., 1999. Intragenic deletion in the gene encoding ubiquitin carboxy-terminal hydrolase in gad mice. Nat. Genet. 23, 47–51.

Sawa, A., Khan, A.A., Hester, L.D., Snyder, S.H., 1997. Glyceraldehyde-3-phosphate dehydrogenase: nuclear translocation participates in neuronal and nonneuronal cell death. Proc. Natl. Acad. Sci. U.S.A. 94, 11669–11674.

Sen, N., Hara, M.R., Kornberg, M.D., Cascio, M.B., Bae, B.I., Shahani, N., Thomas, B., Dawson, T.M., Dawson, V.L., Snyder, S.H., Sawa, A., 2008. Nitric oxide-induced nuclear GAPDH activates p300/CBP and mediates apoptosis. Nat. Cell. Biol. 10, 866–873.

Shaw, M.M., Riederer, B.M., 2003. Sample preparation for two-dimensional gel electrophoresis. Proteomics 3, 1408–1417.

Sirover, M.A., 1999. New insights into an old protein: the functional diversity of mammalian glyceraldehyde-3-phosphate dehydrogenase. Biochim. Biophys. Acta 1432, 159–184.

Stokin, G.B., Lillo, C., Falzone, T.L., Brusch, R.G., Rockenstein, E., Mount, S.L., Raman, R., Davies, P., Masliah, E., Williams, D.S., Goldstein, L.S., 2005. Axonopathy and transport deficits early in the pathogenesis of Alzheimer's disease. Science 307, 1282–1288.

Wang, Y.L., Takeda, A., Osaka, H., Hara, Y., Furuta, A., Setsuie, R., Sun, Y.J., Kwon, J., Sato, Y., Sakurai, M., Noda, M., Yoshikawa, Y., Wada, K., 2004. Accumulation of beta- and gamma-synucleins in the ubiquitin carboxyl-terminal hydrolase L1-deficient gad mouse. Brain Res. 1019, 1–9.

Wilkinson, K.D., Lee, K.M., Deshpande, S., Duerksen-Hughes, P., Boss, J.M., Pohl, J., 1989. The neuron-specific protein PGP 9.5 is a ubiquitin carboxyl-terminal hydrolase. Science 246, 670–673.

Yamazaki, K., Wakasugi, N., Tomita, T., Kikuchi, T., Mukoyama, M., Ando, K., 1988. Gracile axonal dystrophy (GAD), a new neurological mutant in the mouse. Proc. Soc. Exp. Biol. Med. 187, 209–215.

Zheng, L., Roeder, R.G., Luo, Y., 2003. S phase activation of the histone H2B promoter by OCA-S, a coactivator complex that contains GAPDH as a key component. Cell 114, 255–266.

Please cite this article in press as: Goto, A., et al., Proteomic and histochemical analysis of proteins involved in the dying-back-type of axonal degeneration in the gracile axonal dystrophy (*gad*) mouse. Neurochem. Int. (2009), doi:10.1016/j.neuint.2008.12.012

Neurochemistry International xxx (2009) xxx–xxx

Contents lists available at ScienceDirect

Neurochemistry International

journal homepage: www.elsevier.com/locate/neuint

Ubiquitin dimers control the hydrolase activity of UCH-L3

Rieko Setsuie [a], Mikako Sakurai [a,1], Yuriko Sakaguchi [b], Keiji Wada [a,*]

[a] Department of Degenerative Neurological Diseases, National Institute of Neuroscience, National Center of Neurology and Psychiatry, 4-1-1 Ogawahigashi, Kodaira, Tokyo 187-8502, Japan

[b] Department of Chemistry and Biotechnology, Graduate School of Engineering, The University of Tokyo, Bunkyo-ku, Tokyo, Japan

ARTICLE INFO

Article history:
Received 29 September 2008
Received in revised form 3 December 2008
Accepted 15 December 2008

Keywords:
Ubiquitin
Ubiquitin dimer
Ubiquitin carboxy terminal hydrolase-L1 (UCH-L1)
Ubiquitin carboxy terminal hydrolase-L3 (UCH-L3)

ABSTRACT

Ubiquitin (Ub) carboxy terminal hydrolase (UCH)-L1 and UCH-L3 are two of the deubiquitinating enzymes expressed in the brain. Both *gad* mice, which lack UCH-L1 expression and *Uchl3* knockout mice exhibit neurodegeneration, although at distinct areas. These phenotypes indicate the importance of UCH-L1 and UCH-L3 in the regulation of the central nervous system. However, molecular substrates and the molecular regulators of UCH-L1 and UCH-L3 remain poorly identified. Here we show that Ub dimers interact non-covalently with UCH-L3 *in vitro* and in cells. These interactions were not observed with UCH-L1 in cells. *In vitro*, K48-linked Ub dimers pronouncedly inhibited the hydrolase activity of UCH-L3, while mono-Ub, a previously identified interacting protein, inhibited the hydrolase activity of UCH-L1. These results indicate that mono-Ub and Ub dimers may regulate the enzymatic functions of UCH-L1 and UCH-L3, respectively, *in vivo*.

1. Introduction

The ubiquitin (Ub) system is involved in the regulation of various physiological phenomena including development, inflammatory response, and intracellular trafficking (Hershko and Ciechanover, 1998; Hicke, 2001; Glickman and Ciechanover, 2002; Mukhopadhyay and Riezman, 2007). Malfunction of the Ub system in the central nervous system (CNS) may lead to neurodegeneration or synaptic dysfunction (Rubinsztein, 2006; Hegde and Upadhya, 2007). Ub can be covalently conjugated to substrate proteins by the sequential action of E1, E2 and E3 enzymes forming an isopeptide bond between the carboxy terminus of Ub and the lysine residues of the substrates (Hershko and Ciechanover, 1998). The attachment of Ub to the substrates may occur either in the form of a single Ub or a poly-Ub chain, where the carboxy terminus of one Ub moiety is covalently linked to one of the seven Lys residues of an adjacent Ub molecule.

Deubiquitination involves the hydrolysis of the isopeptide bonds between the carboxy terminus glycine of the Ub and the lysine of the substrates or Ub, which requires the activity of deubiquitinating enzymes (DUBs) (Nijman et al., 2005). DUBs can be divided into six distinct families: the Ub-specific processing proteases, the Ub carboxyl-terminal hydrolases (UCHs), the Ataxin-3/Josephin domains, the ovarian tumor domain-containing proteases, the viral processing proteases and the JAMM proteases.

UCH is a cysteine protease with relatively small molecular weight. There is one UCH in yeast, and four UCH isozymes in mammals: UCH-L1, UCH-L3, UCH37 and BAP1. Of these, UCH-L1 and UCH-L3 are the most closely related family members with about 53% identity. These UCHs have also been shown to hydrolyze Nedd8 (neural precursor cell expressed developmentally down regulated 8), a Ub-like protein with 68% identity to Ub (Wada et al., 1998; Hemelaar et al., 2004). The expression of UCH-L3 is ubiquitous whereas that of UCH-L1 is mainly restricted to the brain and the testis/ovary (Wilkinson et al., 1989; Kurihara et al., 2000; Kurihara et al., 2001).

Previous studies using mutant mice of *Uchl1* and *Uchl3* indicated that these enzymes are involved in the regulation of the brain function (Setsuie and Wada, 2007). The I93M point mutation in UCH-L1 is associated with familial Parkinson's disease (Leroy et al., 1998) and we have previously shown that I93M UCH-L1 expression in the cell or in transgenic mice induces dopaminergic neuron death (Setsuie et al., 2007; Kabuta et al., 2008). We also reported that *gad* (gracile axonal dystrophy) mice, which lack Uchl1 expression, show axonal degeneration of the gracile tract, which results in sensory ataxia (Saigoh et al., 1999). Our analysis also indicated that UCH-L1 is involved in many biological aspects including neuronal apoptosis (Harada et al., 2004), neurotransmitter receptor activation (Manago et al., 2005), neural progenitor regulation (Sakurai et al., 2006), learning and memory (Sakurai et al., 2008). On the other hand, UCH-L3 knockout mice show photoreceptor cell degeneration (Semenova

* Corresponding author. Tel.: +81 42 346 1715; fax: +81 42 346 1745.
E-mail address: wada@ncnp.go.jp (K. Wada).

[1] Present address: Department of Pathology and Taub Institute, Columbia University, New York, NY 10032, USA.

0197-0186/$ – see front matter © 2008 Elsevier Ltd. All rights reserved.
doi:10.1016/j.neuint.2008.12.013

Please cite this article in press as: Setsuie, R., et al., Ubiquitin dimers control the hydrolase activity of UCH-L3. Neurochem. Int. (2009), doi:10.1016/j.neuint.2008.12.013

et al., 2003; Sano et al., 2006) and defects in memory function (Wood et al., 2005). These different phenotypes of mutant mice indicate that although both enzymes share similar properties in terms of biochemical identity (Johnston et al., 1997; Larsen et al., 1998; Misaghi et al., 2005; Das et al., 2006), UCH-L1 and UCH-L3 should be differentially controlled or be regulated by distinct molecules.

To identify the proteins that regulate UCH-L1 and UCH-L3 in a diverse manner, we performed immunoaffinity purification assay using UCH-L1 and UCH-L3 and found that UCH-L3 is inhibited by Ub dimers (di-Ub) while UCH-L1 is inhibited by mono-Ub.

2. Experimental procedures

2.1. Isolation and culture of mouse embryonic fibroblasts (MEFs) and their immortalization

Pregnant female *Uchl3* heterozygote mice (Kurihara et al., 2000) were sacrificed at 14–15 days postcoitus. The head, the viscera and the bones of each embryo were removed under a dissecting microscope and a part of these samples were used for genotyping. The remaining portion of embryo was placed in 0.25% trypsin-EDTA (Invitrogen, Carlsbad, CA, USA), cut finely with razor blade, and incubated for 15 min at 37 °C. The cell suspension was passed several times through a 1 ml pipette tip until no clumps were visible. The cell suspension prepared from each individual embryo was washed with medium containing 10% (v/v) fetal bovine serum (FBS). Viable cells were determined by trypan-blue exclusion assay and 4,000,000 viable cells from each embryo were plated in 100 mm culture dishes. MEFs were maintained in Dulbecco's Modified Eagle's Medium (Sigma, St. Louis, MO, USA) supplemented with 10% (v/v) FBS (JRH, Biosciences, Lenexa, KS, USA), 100 U/ml penicillin and streptomycin (Invitrogen). The genotype was determined using the remnants of tissues, and polymerase chain reactions (PCR) were conducted using the primers and the thermal cycling as follows: L3KO-1 primer (5′-ggaactactgagccatatgtgc-3′) L3KO-2 primer (5′-cggacttactccatcacttcac-3′) L3KO-3 primer (5′-cttgtgagcgccaagtgc-3′), one cycle of 98 °C for 5 min, 30 cycles at 98 °C for 10 s, 60 °C for 20 s, and 72 °C for 30 s. For the immortalization of MEFs, basic 3T3 protocols were carried out as described (Todaro and Green, 1963).

2.2. Construction of cell lines expressing human wild-type or mutant UCH-L3

Retrovirus vectors encoding human wild-type UCH-L3 were constructed as follows. Full-length human UCH-L3 cDNA was cloned from human liver cDNA library and inserted into the pGEM-T vector (Promega, Madison, WI, USA). For PCR-based amplification of the insert, the huchl3-retro-s2 primer (5′-GGGGCTCGAGCGCGG-CATGGAGGGTCAACGCTGGCT-3′) and huchl3-pci-as1 primer (5′-GGGGGCGGCC-GCCTATGCTGCAGAAAGAGC AATCG-3′) were used with 35 cycles of 94 °C for 30 s, 55 °C for 30 s and 72 °C for 1 min. The amplified PCR fragment and pOZ-N retrovirus vector were successively digested with XhoI and NotI. The enzymatically digested PCR fragment and pOZ-N vector were subsequently applied to electrophoresis, gel extraction and ligated using the ligation system ver2 (Takara, Tokyo, Japan). This resulted in the insertion of human UCH-L3 without a starting methionine after the HA and FLAG double-tag sequence between the XhoI and NotI sites at the multicloning site of the pOZ-N double-tag retrovirus vector. To obtain Ub hydrolase-deficient C95S mutant- and Ub affinity deficient D33A mutant-encoding retrovirus vectors, the Cys95 or Asp33 of hUCH-L3 were mutated to Ser or Ala, respectively, using PCR-based *in vitro* mutagenesis (Stratagene, La Jolla, CA, USA). The primers used for mutagenesis were huchl3-C95S-s1 (5′-ATCAGCAATGCAATGCCTGTGGAAC AATTGGA-3′), hchl3-C95S-as1 (5′-TCCAATTGTTCCACAGGCATTGCTGAT-3′), huchl3-D33A-s (5′-CTAACT-GGCAATTCGTTGCTGTATATGGAATGGATCC TGAAC-3′) and huchl3-D33A-as (5′-GTTCAGGATCCATTCCATATA CAGCAACGAATTGCCAGTTAG-3′). The human UHCL1 or GFP cDNA derived inserts were cloned into the XhoI and NotI site of the same retrovirus vector, as described previously (Sakurai et al., 2006). The production of retroviruses and cell lines were conducted as described elsewhere (Ogawa et al., 2002).

2.3. Immunoprecipitation

2.5×10^8 floating Hela cells expressing FLAG-HA tagged hUCH-L3 were collected and washed with phosphate buffered saline (PBS) twice and the cell pellets were stored at −80 °C until all of the clones were ready for lysis. The floating Hela cells were quickly thawed at 37 °C, suspended in 15 ml of ice-cold modified RIPA buffer (50 mM Tris–HCl (pH 7.4), 1% Nonidet P40, 0.25% sodium deoxycholate, 150 mM NaCl, 1 mM EDTA, 1 mM $NaVO_4$, 1 mM NaF with Complete EDTA-free protease inhibitors (Roche Diagnostics, Indianapolis, IN, USA)), and kept on ice for 30 min. After three repeated sonications for 10 s with 30 s intervals, lysates were centrifuged at 12,000 rpm at 4 °C for 10 min using a swing-rotor type centrifuge. The supernatant was recovered for further purification and aliquots were kept at −80 °C as a pre-immunoprecipitation lysate. To the remaining supernatant, anti-FLAG M2 antibody-conjugated agarose (Sigma) in 600 μl slurry was added and gently rotated at 4 °C for 8 h. After rotation, the samples were poured into the empty column (Bio-Rad, Hercules, CA, USA), washed four times with 8 ml 0.1 B buffer (20 mM Tris–HCl (pH 8.0), 0.1 M KCl, 5 mM $MgCl_2$, 10% glycerol, 0.1% Tween-20, 10 mM β-mercaptoethanol, 0.2 mM PMSF), and briefly centrifuged to remove the excess washing buffer. After capping the bottom of the column, 600 μl elution buffer (160 μg/ml of 3 × FLAG peptide in 0.1 B buffer) were added to the column, rotated at 4 °C for 1 h, and eluted into an eppendorf tube. This elution step was repeated and a total of 1.2 ml eluate was used for the second purification. The second purification was performed using the anti-HA antibody (clone 12CA5)-conjugated agarose. The steps were the same as for FLAG purification except that the scale was minimized with 100 μl of elution (1 mg/ml HA peptide (Roche) in 0.1 B buffer). The resulting final eluates were kept at −80 °C until analysis.

2.4. Mass spectrometry analysis

After the negative staining (Nakalai Tesque Inc., Kyoto, Japan) of the SDS-PAGE gels, protein bands were sliced from the gel, reduced, S-alkylated, and subjected to in-gel trypsin digestion. The digested peptides were extracted with 50% acetonitrile and 0.1% trifluoroacetic acid and subjected to liquid-chromatography tandem mass spectrometry (LC–MS/MS) analysis.

2.5. Silver staining and Western blotting

Silver staining was done using the Daiichi Silver staining Kit (Daiichi, Tokyo, Japan). For the Western blotting of UCH-L3 or HA-FLAG tagged UCH-L3, 15% mini gels (DRC, Tokyo, Japan) were used. For the detection of mono- or di-Ub, or Nedd8, 15–20% gradient mini gels (DRC) were used. For 2D-Western blotting, samples were loaded on 4–11 N IPG strips (GE Healthcare UK Ltd., Buckinghamshire, England) using IPGphor and the second dimension was run on 15–20% gradient gels (DRC). The antibodies used were anti-HA antibody (clone 12CA5, 1:1,000), anti-FLAG M2 antibody (Sigma; 1:1000), anti-Ub antibody (Sigma; 1:1000 or Dako; 1:1000), anti-Nedd8 antibody (Cell signaling; 1:1000) anti-UCH-L1 antibody (Ultraclone RA95101; 1:5000, England, UK) and anti-UCH-L3 antibody ((Kwon et al., 2004); 1:1,000). HRP-conjugated secondary antibodies were from Pierce and signals were detected using a chemiluminescent Super Signal West Dura Extended Duration Substrate kit or West Femto Maximum Sensitivity Substrate kit (Pierce, Rochford, IL) and analyzed with a Chemilmager (Alpha Innotech, San Leandro, CA). The protein marker was purchased from Bio-Rad.

2.6. Pull-down assay

6HN-tagged human UCH-L3 and UCH-L1 proteins were prepared as described previously (Nishikawa et al., 2003). Pull-down assay was conducted as described previously with some modifications (Kabuta et al., 2008). In brief, 6 μg 6HN-UCH and 4 μg of either K48-linked di-Ub, K63-linked di-Ub, or linear di-Ub (all from Boston Biochem, Cambrige, MA, USA), were mixed in the presence of 0.1 μg/ml BSA in tris-buffered saline (TBS) at 4 °C for 2 h. Fifty micro liters of TALON resin (Clontech, Palo Alto, CA, USA) were added to samples and incubated at 4 °C for 1 h. After washing the resin five times with PBS in the presence of 20 mM imidazole and 0.05% Tween-20, the bound proteins were eluted with SDS sample buffer.

2.7. Ubiquitin hydrolase activity assay

The Ub hydrolase activity assay, using recombinant UCH-L3 and Ub-AMC (both from Boston Biochem), was performed as described previously (Nishikawa et al., 2003), in the presence or absence of di-Ub.

3. Results

3.1. UCH-L3 but not UCH-L1 interacts with di-Ub

To identify the proteins that interact with UCH-L1 or UCH-L3, which might represent the potential substrates or the functional effecters, we performed immunoaffinity chromatography. Floating Hela cells that stably expressed human UCH-L3 tagged with the FLAG-HA epitope at its N-terminus (L3 WT), UCH-L3 C95S (active site mutant of UCH-L3), UCH-L1 (L1 WT), UCH-L1 C90S (active site mutant of UCH-L1), GFP and Mock were constructed (Fig. 1A). Western blotting using anti-HA and anti-FLAG antibodies detected a single band at the appropriate molecular weight in each cell line indicating FLAG-HA tagged proteins were sufficiently expressed and at comparable levels (Fig. 1A). We detected two bands with the anti-UCH-L3 antibody in all of the cell lines; these bands correspond to the exogenously expressed and endogenously expressed UCH-L3 in Hela cells (Fig. 1A).

Please cite this article in press as: Setsuie, R., et al., Ubiquitin dimers control the hydrolase activity of UCH-L3. Neurochem. Int. (2009), doi:10.1016/j.neuint.2008.12.013

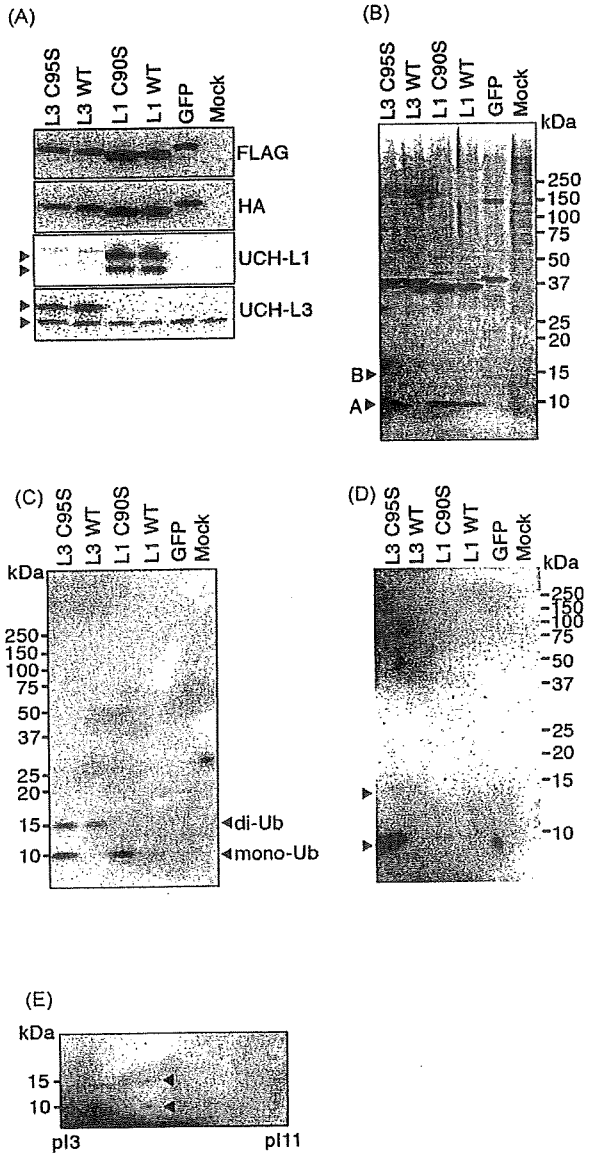

Fig. 1. Di-Ub interacts with UCH-L3. (A) Floating Hela cells stably expressing FLAG-HA double-tagged UCH-L3 or UCH-L1 were constructed. The expression of exogenous UCH-L3 or UCH-L1 was confirmed by anti-FLAG, anti-HA, anti-UCH-L1 and anti-UCH-L3 antibodies. Anti-UCH-L1 antibody showed two bands (indicated by the arrows), where upper band corresponds to the predicted molecular weight of UCH-L1 including FLAG-HA tag at the N-terminal. The lower band may indicate the N-terminally processed form of UCH-L1, which lack FLAG-HA tag. Anti-UCH-L3 antibody also showed two bands, where lower band represent the endogenous UCH-L3 expressed in Hela cells. (B) Silver staining of proteins, which are obtained by the sequential immunoaffinity purification using anti-FLAG antibody-conjugated agarose and anti-HA antibody-conjugated agarose. The bands, which are indicated by the arrow A and B were excised and processed for LC–MS/MS analysis. (C) Western blotting of the proteins as in (B) with anti-Ub antibody from Sigma–Aldrich. Note the presence of anti-Ub antibody immunoreactive bands at about 10 kDa and 15 kDa, which represent mono- and di-Ub. (D) Western blotting of the proteins as in (B) with anti-Nedd8 antibody from Cell Signaling. Note the presence of anti-Nedd8 antibody immunoreactive bands at about 10 kDa and 15 kDa, which may represent mono- and di-Nedd8. (E) 2D-Western blotting of the proteins, which is obtained by the sequential immunoaffinity purification of UCH-L3 C95S expressing Hela cell lysate as in (B). Anti-Ub antibody from Sigma–Aldrich is used.

UCH-L1- or UCH-L3-containing complexes were affinity purified from stable cells using anti-FLAG antibody-conjugated agarose, followed by anti-HA antibody-conjugated agarose and each elution was conducted under native conditions using 3×

Table 1
The amino acid sequences of fragments detected by the mass spectrometric analysis of bands A and B from Fig. 1B.

Band	Amino acid sequences
A	MQIFVKTLTG KTITLEVEPS DTIENVKAKI QDKEGIPPDQ QRLIFAGKQL EDGRTLSDYN IQKESTLHLV LRLRGG
B	MQIFVKTLTG KTITLEVEPS DTIENVKAKI QDKEGIPPDQ QRLIFAGKQL EDGRTLSDYN IQKESTLHLV LRLRGG

The bands, from the immunoaffinity-purified complex of C95S mutant corresponding to A and B of Fig. 1B, are excised and subjected to LC–MS/MS analysis as described in the Section 2, and the amino acid sequences in red are detected fragments by LC–MS/MS analysis.

FLAG peptide or HA peptide. After the second immunoaffinity chromatography, proteins associated with UCH-L3 WT, UCH-L3 C95S, UCH-L1 WT and UCH-L1 C90S were identified by SDS-PAGE followed by silver staining (Fig. 1B). The deduced amino acid sequences, which were obtained from the LC–MS/MS analysis, indicate that the bands with a molecular weight of about 9 kDa (arrow A) in Fig. 1B correspond to the free mono-Ub (Table 1). Consistently, the immunoblotting of immunoaffinity-purified proteins with anti-Ub antibody, which recognizes both free Ub and ubiquitylated proteins, revealed that these bands represent free mono-Ub (Fig. 1C). The finding that UCH-L1 and the UCH-L1 C90S mutant have strong affinity for mono-Ub is consistent with our previous finding that UCH-L1 interacts with and stabilizes free mono-Ub *in vivo* (Osaka et al., 2003). The strong detection of mono-Ub with the UCH-L3 C95S mutant complex but not with the UCH-L3 WT complex indicates that C95S mutation leads to either the conformational change resulting in the strong interaction with mono-Ub, or the lack of hydrolase activity that results in the interaction with the substrate.

The molecule with molecular weight of about 15 kDa (arrow B in Fig. 1B) identified for the UCH-L3 WT and UCH-L3 C95S immunoaffinity-purified proteins, and which had Ub sequence within this molecule, was of interest because this molecule was specific to UCH-L3 and not UCH-L1. Although the molecular weight is greater than for free mono-Ub, LC–MS/MS analysis of this band only revealed Ub (Table 1). It is known that free di-Ub has a size of about 15 kDa. To confirm whether the bands at 15 kDa (arrow B in Fig. 1B) are, in fact, free di-Ub, we performed 2D-Western blotting of the C95S immunoaffinity-purified complex using the anti-Ub antibody. The p*I* of di-Ub should be similar to that of mono-Ub. As shown in Fig. 1E, the 15 kDa molecule (upper arrow in Fig. 1E) had a p*I* similar to that of free mono-Ub (lower arrow in Fig. 1E), indicating that the band may represent di-Ub.

To confirm the direct interaction of di-Ub and UCH-L3, we performed pull-down assays using recombinant mono-Ub or di-Ub and UCH-L3. As shown in Fig. 2B, UCH-L3 can form physiological complexes not only with di-Ub but also with mono-Ub. However, the affinity of UCH-L3 to mono-Ub is weak compared to di-Ub (see Fig. 1B, C and Fig. 2A).

Nedd8, an Ub-like protein with 57% identity to Ub, is a previously reported UCH-L3 and UCH-L1 interacting protein (Wada et al., 1998; Hemelaar et al., 2004). Although we did not detect any derivatives of Nedd8 on LC–MS/MS analysis, Western blotting analysis of immunoaffinity-purified complexes using the anti-Nedd8 antibody revealed several bands, which presumably represent mono-Nedd8 (lower arrow in Fig. 1D) and di-Nedd8 (upper arrow in Fig. 1D).

Please cite this article in press as: Setsuie, R., et al., Ubiquitin dimers control the hydrolase activity of UCH-L3. Neurochem. Int. (2009), doi:10.1016/j.neuint.2008.12.013

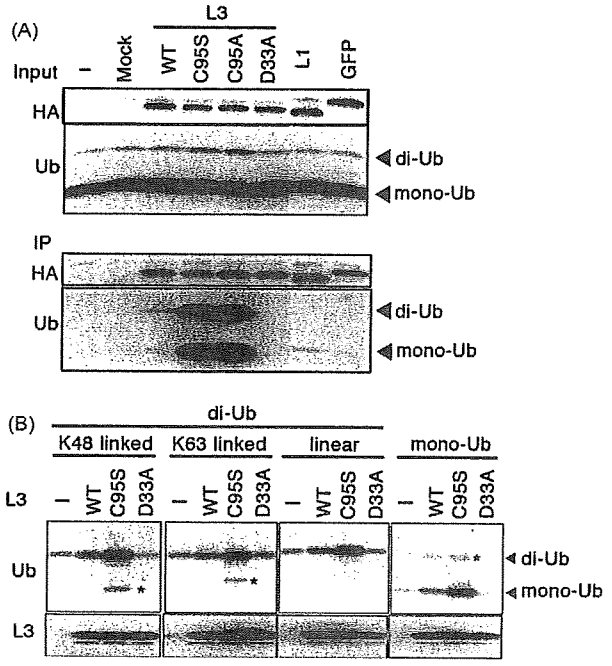

Fig. 2. C95 and D33 of UCH-L3 are involved in the interaction with K48-linked, or K63-linked or linear di-Ub. (A) UCH-L3 interacting proteins were co-immunoprecipitated from Hela cells expressing FLAG-HA tagged UCH-L3 mutants. Cell lysates were immunoprecipitated using anti-HA antibody and co-immunoprecepitates were analyzed by anti-Ub antibody from Sigma–Aldrich. Note the presence of di-Ub in UCH-L3 WT or C95S mutant or C95A mutant immunoprecipitates but not in UCH-L3 D33A mutant or UCH-L1 immunoprecipitates. (B) *In vitro* pull-down assays using recombinant UCH-L3 and recombinant di-Ub or mono-Ub. The pulled-down samples were analyzed by anti-UCH-L3 antibody and anti-Ub antibody from DAKO. UCH-L3 WT and C95S mutant interacted with K48-linked, or K63-linked or linear di-Ub or mono-Ub while these interactions were diminished with D33A mutant. The bands with the asterisks are unidentified molecules, which is presumably derived from the contaminants of di-Ub or mono-Ub.

3.2. Di-ubiquitin interacts directly with UCH-L3 via hydrolytic active site

NMR studies and X-ray studies of UCHs complexed with Ub derivatives indicated that D33 of UCH-L3 is important for its affinity to Ub (Wilkinson et al., 1999; Misaghi et al., 2005). To confirm whether this amino acid is also responsible for the interaction of di-Ub with UCH-L3, we performed an immunoprecipitation assay using mutant UCH-L3. FLAG-HA tagged UCH-L3 WT, C95S, C95A, D33A mutants and UCH-L1 expressing Hela cells were immunoprecipitated with anti-HA antibody-conjugated agarose. As shown in Fig. 2A, the D33A mutation diminished the interaction of di-Ub with UCH-L3 while the C95S and the C95A mutations enhanced the interaction.

The first methionine and seven internal lysine residues of Ub are known to form isopeptide bonds with the carboxy terminus glycine of an adjacent Ub molecule (Kirkpatrick et al., 2005; Kirisako et al., 2006). Thus, eight various forms of di-Ub may exist. However, only K48 and K63-linked di-Ub are presumed to exist with relative abundance *in vivo* with the former being identified *in vivo* (van Nocker and Vierstra, 1993; Hochstrasser, 2006). In addition, previous studies raised the possibility that tandemly conjugated di-Ub may form after processing of the Ub gene products by the DUBs (Wilkinson, 1997). Thus, we assessed whether these di-Ubs (linear, K48-linked and K63-linked) can interact with UCH-L3 *in vitro*. The pull-down analysis of di-Ub with 6HN-tagged UCH-L3 indicated that the K48-linked, K63-linked and linear di-Ub all interacted with UCH-L3 (Fig. 2B). In addition, the pull-down analysis of di-Ub using the D33A mutant abolished the interaction, while the C95S mutant increased the interaction. These results also indicate that D33 and C95 of UCH-L3 are amino acid residues that are involved in the interaction with di-Ub.

3.3. Exogenously expressed UCH-L3 does not hydrolyze di-Ub in cells

We have shown that UCH-L3 interacts with free di-Ub. The previous *in vitro* studies using recombinant human UCH-L3 showed that UCH-L3 neither have the activity toward hydrolyzing tandemly conjugated di-Ub or K48-linked di-Ub though it can hydrolyze Ub conjugates with small adducts less than 20 amino acids or nucleophils such as glutathione (Larsen et al., 1998). To confirm that di-Ubs are not the substrate of UCH-L3, we also performed hydrolase assays using K48-linked, K63-linked and linear di-Ub as the substrates *in vitro*. After incubation for 24 h, UCH-L3 did not produce mono-Ub from these three forms of di-Ub (data not shown), which is consistent with previous reports (Larsen et al., 1998). Although UCH-L3 did not show hydrolase activity toward the K48-linked, K63-linked or linear di-Ub, there exists the possibility that other forms of di-Ub (presumably K11-linked, K27-linked, K29-linked and K33-linked di-Ubs) may be hydrolyzed by UCH-L3. To eliminate this possibility, we analyzed stable cell lines expressing several functional mutants of UCH-L3 and determined whether di-Ub accumulates in the absence of UCH-L3 hydrolase activity.

Two immortalized 3T3 cell lines derived from two different UCH-L3 knockout mouse embryonic fibroblasts were generated and used to make stable cell lines either expressing WT UCH-L3, its mutants C95S, D33A, UCH-L1 or GFP. The same retrovirus systems were used as in Fig. 1, resulting in the attachment of FLAG-HA tags to each exogenous protein. Cell lysates were immunoblotted using anti-HA, anti-UCH-L1, and anti-UCH-L3 antibodies (Fig. 3A). The absence of endogenous UCH-L1 or UCH-L3 and the presence of exogenous proteins at comparable levels were assessed in these cells (Fig. 3A). The immunoprecipitation assays of several UCH-L3 mutants indicated that the D33A mutant lost the affinity to interact with di-Ub while the C95S mutant retained this function (Fig. 2A). In this condition, immunoblotting with the anti-Ub antibody was performed. We presumed that, if UCH-L3 functions to hydrolyze free di-Ub *in vivo*, the free di-Ub would accumulate in cells not expressing the WT UCH-L3. However, cells expressing WT UCH-L3 showed increasing levels of free di-Ub compared with the Mock- or GFP-expressing cells (Fig. 3A and B). Moreover, the D33A mutant-expressing cells did not show any signs of free di-Ub accumulation (Fig. 3A and B). In addition, lack of UCH-L3 expression in the tissues or MEF cells derived from Uchl3 knockout mice indicated no signs of di-Ub accumulation (Fig. 3C and data not shown). These results indicate that UCH-L3 does not function to hydrolyze free di-Ub.

3.4. Endogenous UCH-L3 does not show stabilizing effects on mono or di-Ub in cells or tissues

We have already shown that UCH-L1 interacts with and stabilizes mono-Ub *in vivo* (Osaka et al., 2003). The increased levels of free mono-Ub and di-Ub in the cells expressing WT and C95S mutant UCH-L3 in the immortalized 3T3 KO cells (Fig. 3A and B) prompted us to speculate that UCH-L3 might stabilize mono- and di-Ub *in vivo*. Thus, we compared the protein levels of mono- and di-Ub in various tissues from wild-type mice and knockout mice using Western blotting analysis with the anti-Ub antibody. As shown in Fig. 3C, tissues (including the testis where UCH-L3 expression is most abundant) of knockout mice did not show reduced mono-Ub or di-Ub levels. This result indicates that, at least in the tissues analyzed, UCH-L3 is not involved in the stabilization of di-Ub *in vivo*.

Please cite this article in press as: Setsuie, R., et al., Ubiquitin dimers control the hydrolase activity of UCH-L3. Neurochem. Int. (2009), doi:10.1016/j.neuint.2008.12.013

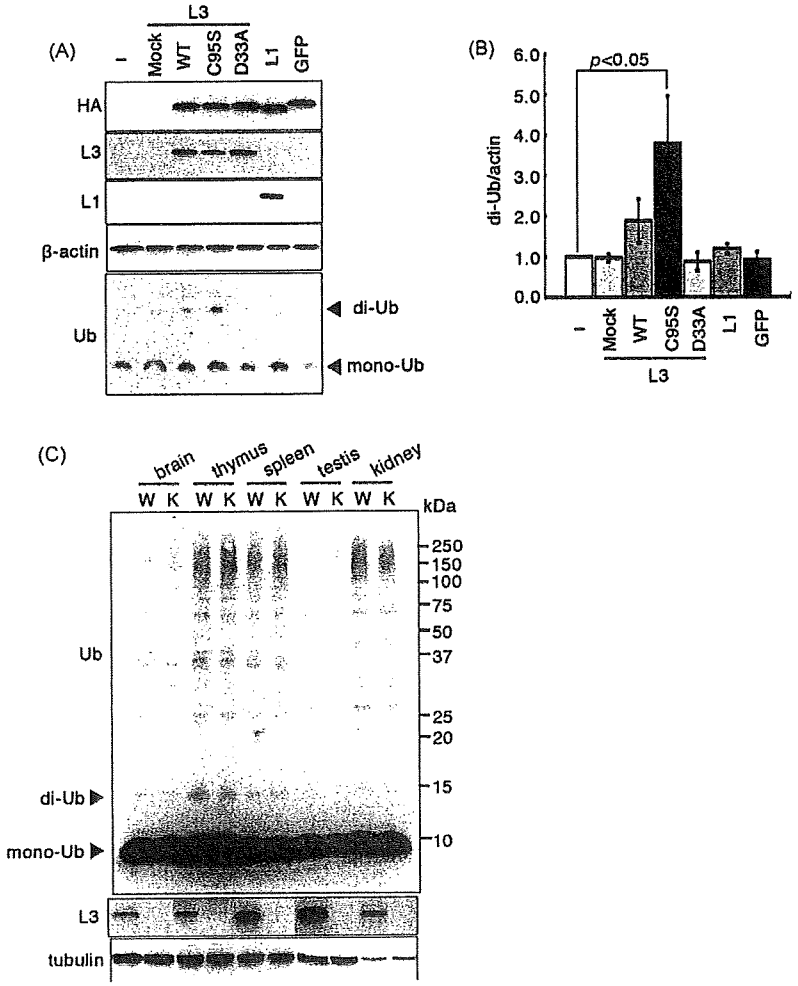

Fig. 3. UCH-L3 does not hydrolyze nor stabilize di-Ub *in vivo*. (A) The Western blotting analysis of immortalized MEF cells derived from Uchl3 knockout mice, which express FLAG-HA tagged UCH-L3 mutants. Note that these cells lack the expression of endogenous UCH-L3. (B) The quantitative analysis of bands corresponding to di-Ub in (A). The experiments were done three times and the statistical analysis was conducted by ANOVA followed by Dunnet's test. Data are mean ± S.E.M, $P < 0.05$. (C) Western blotting analysis of the tissues (whole brain, thymus, spleen, testis and kidney) from Uchl3 knockout (KO) mice and his wild-type littermate (WT) using anti-Ub antibody from Dako. Testis and spleen were included because these tissues express UCH-L3 most abundantly.

3.5. Di-Ub and mono-Ub inhibit the hydrolase activities of both UCH-L3 and UCH-L1

As shown in Fig. 2A and B, D33 and C95 of UCH-L3 are involved in the interaction with di-Ub. C95 is part of the active site triad of proteases and D33 is an essential amino acid for the interaction with Ub-aldehyde or Ub-vinylmethylsulfone (Wilkinson et al., 1999; Misaghi et al., 2005). Thus, we speculated that di-Ub might inhibit the enzymatic activity of UCH-L3. We performed *in vitro* hydrolase activity assays using Ub-AMC as the model substrate in the presence and absence of K48-linked, K63-linked and tandemly linked di-Ub and mono-Ub. As shown in Fig. 4A–C, the hydrolase activity of UCH-L3 is significantly inhibited in the presence of all forms of di-Ub and mono-Ub with the most prominent effect observed with the K48-linked di-Ub (about 60% inhibition). Meanwhile, mono-Ub as well as K48-linked di-Ub showed a significant inhibitory effect on the hydrolase activity of UCH-L1 (about 60% and 45% inhibition, respectively) (Fig. 4D).

4. Discussion

Our immunoaffinity purification assay coupled with LC–MS/MS analysis of Hela cells stably expressing exogenous UCH-L3 and UCH-L1 revealed that UCH-L3, but not its closest isozyme UCH-L1, interacts with di-Ub. Interaction with mono-Ub, an important physiological interacting partner of UCH-L1, was not observed with WT UCH-L3 in cells (Fig. 1). Structure analysis by X-ray crystallography and NMR spectroscopy indicated that important amino acids for the interaction of Ub-aldehyde or Ub-vinylmethylester, with UCH-L1 and UCH-L3 are all conserved in these two enzymes (Wilkinson et al., 1999; Misaghi et al., 2005). However, these enzymes share only 53% amino acid identity with different affinities for mono- and di-Ub (Figs. 1 and 2). In addition, the enzymatic activity toward the artificial Ub substrate (Ub-AMC) differs significantly between UCH-L1 and UCH-L3; UCH-L1 activity (Kcat) is less then 1/200 that of UCH-L3 (Liu et al., 2002). The amino acid sequences, which are not conserved among these UCHs should be responsible for these different characteristics.

Analysis of the UCH-L3 mutant revealed that D33 and C95 are essential for the interaction with di-Ub (Fig. 2). The previous kinetic analysis, NMR analysis and X-ray analysis revealed that C95 is an active site and D33 reside within the enzymatic catalytic pocket of UCH-L3 (Larsen et al., 1996; Johnston et al., 1997; Wilkinson et al., 1999; Misaghi et al., 2005). The carboxy terminal moiety of Ub in the ubiquitinated substrate penetrates this catalytic pocket of UCH-L3 and D33 of UCH-L3 forms a salt bridge

Please cite this article in press as: Setsuie, R., et al., Ubiquitin dimers control the hydrolase activity of UCH-L3. Neurochem. Int. (2009), doi:10.1016/j.neuint.2008.12.013

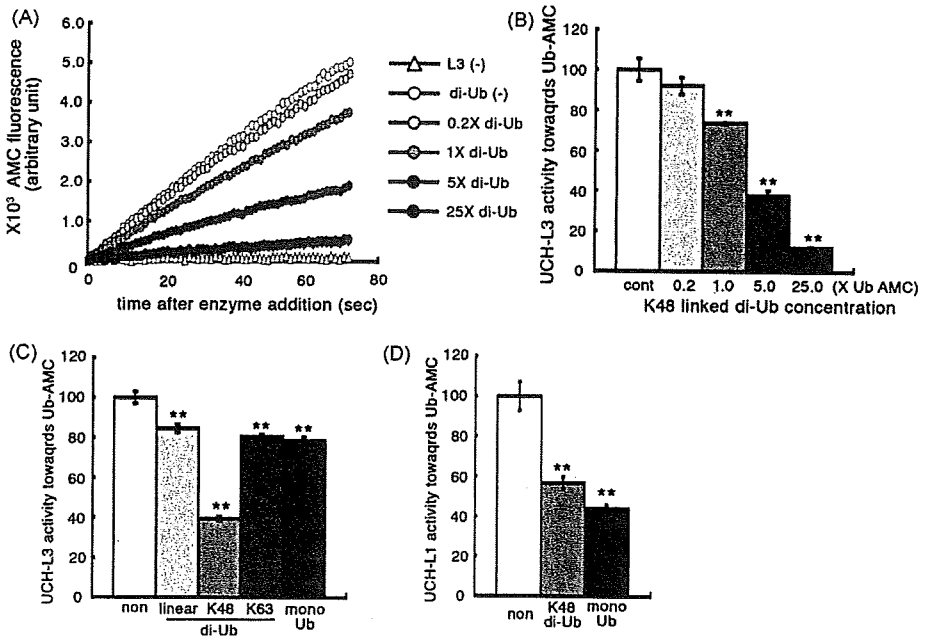

Fig. 4. Di-Ub inhibits UCH-L3 deubiquitinating activity while mono-Ub inhibits UCH-L1 deubiquitinating activity *in vitro*. (A) The kinetic curves of UCH-L3 in the presence or absence of K48-linked di-Ub. 0.2X or 1X or 5X or 25X moles of di-Ub compared to Ub-AMC substrate were included in the reaction. (B) The kinetic analysis of (A). (C) UCH-L3 deubiquitinating activity in the presence or absence of K48-linked or K63-linked or linear di-Ub or mono-Ub as in (B). 5X moles of di-Ub or mono-Ub compared to Ub-AMC substrate were included in the reaction. (D) UCH-L1 deubiquitinating activity in the presence or absence of K48-linked di-Ub or mono-Ub as in (B). 5X moles of di-Ub or mono-Ub compared to Ub-AMC substrate were included in the reaction. All statistical analyses were conducted by ANOVA followed by Dunnet's test. Data are mean ± S.E.M. ($n = 4$) $^{**}p < 0.001$ vs controls.

with R72 of Ub. The active site cysteine and an acidic residue corresponding to C95 and D33 of UCH-L3 are conserved among all UCH family proteins including UCH-L1 (Wilkinson et al., 1999; Misaghi et al., 2005). Thus, the interactions of di-Ub with UCH-L3 and mono-Ub with UCH-L1 occupy the catalytic centers of UCH-L3, and UCH-L1, respectively.

One of the physiological functions of UCH-L1 is to interact with mono-Ub and to protect mono-Ub from degradation (Osaka et al., 2003). This function was confirmed using *gad* mice and nm3419 mutant mice, which lack UCH-L1 protein expression. The protein level of free mono-Ub in the brain stem or the sciatic nerve, the site where *gad* mice are most severely affected, was prominently decreased in the *gad* mice compared with controls. In addition, cerebrum of nm3418 mutant mice also contained decreased levels of mono-Ub compared to that of control mice (Walters et al., 2008). Likewise, UCH-L3 might interact with di-Ub to protect it from degradation. To confirm this possibility, we compared the protein level of di-Ub in several tissues of UCH-L3 knockout mice with that of wild-type mice. In contrast with our expectations, none of the tissues derived from the knockout mice showed lower di-Ub levels (Fig. 3C). However, the exogenous expression of UCH-L3 in 3T3 immortalized mouse embryonic fibroblast, derived from the UCH-L3 knockout mice, revealed that its expression up-regulated the protein level of di-Ub, while the D33A mutant, a mutant that lacks the ability to interact with di-Ub, did not show this effect (Fig. 3A and B). Thus, we cannot exclude the possibility that, under some conditions, UCH-L3 may interact with di-Ub to protect it from degradation.

Previous biochemical analysis indicated that UCH-L3 is unable to hydrolyze tandemly conjugated di-Ub or K48-linked di-Ub (Larsen et al., 1998). To confirm that UCH-L3 is not capable of hydrolyzing di-Ub, we also performed *in vitro* enzymatic assays using K48-linked, and K63-linked di-Ub. We choose these two forms of di-Ub, among the eight possible linkages because these two forms of di-Ub are known to exist at relatively high levels *in vivo* (van Nocker and Vierstra, 1993; Hochstrasser, 2006). Consistent with the previous reports (Larsen et al., 1998), neither form of di-Ub was hydrolyzed by UCH-L3 even after 24 h incubation (data not shown). Thus, di-Ub is unlikely to be a substrate of UCH-L3.

Because the mutant analysis indicated that the catalytic pocket of UCH-L3 is affected by the interaction with di-Ub, another functional explanation of di-Ub interaction with UCH-L3 is that it might inhibit enzymatic activity. Indeed, the addition of K48-linked, K63-linked, and tandemly conjugated di-Ub, as well as mono-Ub showed inhibitory effects on hydrolyzing Ub-AMC (Fig. 4C). Of these three forms of di-Ub and mono-Ub, K48-linked di-Ub showed the most prominent inhibitory effect toward UCH-L3. A previous report indicated that nonhydrolyzable di-Ub analogues can inhibit Ub hydrolase activity of UCH-L3 where its activity was monitored by Ub-AMC (Yin et al., 2000). UCH-L3 was inhibited approximately equally by mono-Ub and di-Ub analogues linked through residues 11, 29, 48 (Kis of 200, 151, 199, and 107 μM, respectively) and the dimer analogue linked through residues 63 and 76 (head-to-head tandem conjugation) with a Ki of 13 μM (Yin et al., 2000). In addition, it has been reported that K48-linked di-Ub is the most abundant of all eight forms of di-Ub in tissues and cells. Thus, our results indicate that K48-linked di-Ub can function as an endogenous UCH-L3 inhibitor. Furthermore, we also found that addition of mono-Ub as well as K48-linked di-Ub inhibited the enzymatic activity of UCH-L1 (Fig. 4D). As UCH-L1 preferentially interacts with mono-Ub and the protein level of mono-Ub is high compared to di-Ubs in the cell, mono-Ub can function as endogenous inhibitor of UCH-L1. Together, these results indicate that di-Ub and mono-Ub regulate the enzymatic activity of UCH-L3 and UCH-L1, respectively.

In addition to Ub, UCH-L1 and UCH-L3 show affinity for Nedd8, an Ub-like protein, which shares 63% amino acid identity with Ub. Thus, these enzymes are thought to possess dual enzymatic activity toward the Ub and Nedd8 substrates. Although we could

Please cite this article in press as: Setsuie, R., et al., Ubiquitin dimers control the hydrolase activity of UCH-L3. Neurochem. Int. (2009), doi:10.1016/j.neuint.2008.12.013

not detect any types of Nedd8 derivatives in LC–MS/MS analysis, the Western blotting analysis of immunoaffinity-purified complexes with the Nedd8 specific antibody revealed several bands (Fig. 1D). The predicted molecular size of these bands indicates that UCH-L1 may interact with mono-Nedd8 while UCH-L3 may interact with di-Nedd8. UCHs are reported to show only weak affinity for Nedd8 compared with Ub. In addition, the expression level of Nedd8 protein is presumably low compared with that of Ub. These two differences might account for the limited amount of Nedd8 derivatives in the immunoaffinity-purified complex that can only be detected by Western blotting analysis. These interactions need to be further analyzed.

In conclusion, our analyses indicate that the major interacting partner of UCH-L1 is mono-Ub while that of UCH-L3 is di-Ub. These interactions appear to be responsible for the inhibition of deubiquitinating activity.

Acknowledgements

This work was supported by grants-in-aid for scientific research from the Japan Society for the Promotion of Science; a research grant in priority area research from the Ministry of Education, Culture, Sports, Science, and Technology, Japan; grants-in-aid for scientific research from the Ministry of Health, Labor, and Welfare, Japan; and the Program for Promotion of Fundamental Studies in Health Sciences of the National Institute of Biomedical Innovation and the New Energy and Industrial Technology Development Organization, Japan.

The authors thank Yoshihiro Nakatani and Hidesato Ogawa for providing the retroviral expression system and immunoaffinity purification system; Hiromi Fujita for the care and breeding of animals; Mari Suzuki, Yukihiro Tsuchiya, Tomohiro Kabuta and Yasuyuki Suzuki for valuable discussions.

References

Das, C., Hoang, Q.Q., Kreinbring, C.A., Luchansky, S.J., Meray, R.K., Ray, S.S., Lansbury, P.T., Ringe, D., Petsko, G.A., 2006. Structural basis for conformational plasticity of the Parkinson's disease-associated ubiquitin hydrolase UCH-L1. Proc. Natl. Acad. Sci. U. S. A. 103, 4675–4680.

Glickman, M.H., Ciechanover, A., 2002. The ubiquitin-proteasome proteolytic pathway: destruction for the sake of construction. Physiol. Rev. 82, 373–428.

Harada, T., Harada, C., Wang, Y.L., Osaka, H., Amanai, K., Tanaka, K., Takizawa, S., Setsuie, R., Sakurai, M., Sato, Y., Noda, M., Wada, K., 2004. Role of ubiquitin carboxy terminal hydrolase-L1 in neural cell apoptosis induced by ischemic retinal injury in vivo. Am. J. Pathol. 164, 59–64.

Hegde, A., Upadhya, S., 2007. The ubiquitin–proteasome pathway in health and disease of the nervous system. Trends Neurosci. 30, 587–595.

Hemelaar, J., Borodovsky, A., Kessler, B.M., Reverter, D., Cook, J., Kolli, N., Gan-Erdene, T., Wilkinson, K.D., Gill, G., Lima, C.D., Ploegh, H.L., Ovaa, H., 2004. Specific and covalent targeting of conjugating and deconjugating enzymes of ubiquitin-like proteins. Mol. Cell Biol. 24, 84–95.

Hershko, A., Ciechanover, A., 1998. The ubiquitin system. Annu. Rev. Biochem. 67, 425–479.

Hicke, L., 2001. Protein regulation by monoubiquitin. Nat. Rev. Mol. Cell Biol. 2, 195–201.

Hochstrasser, M., 2006. Lingering mysteries of ubiquitin-chain assembly. Cell 124, 27–34.

Johnston, S.C., Larsen, C.N., Cook, W.J., Wilkinson, K.D., Hill, C.P., 1997. Crystal structure of a deubiquitinating enzyme (human UCH-L3) at 1,8 A resolution. Embo J. 16, 3787–3796.

Kabuta, T., Setsuie, R., Mitsui, T., Kinugawa, A., Sakurai, M., Aoki, S., Uchida, K., Wada, K., 2008. Aberrant molecular properties shared by familial Parkinson's disease-associated mutant UCH-L1 and carbonyl-modified UCH-L1. Hum. Mol. Genet. 17, 1482–1496.

Kirisako, T., Kamei, K., Murata, S., Kato, M., Fukumoto, H., Kanie, M., Sano, S., Tokunaga, F., Tanaka, K., Iwai, K., 2006. A ubiquitin ligase complex assembles linear polyubiquitin chains. Embo J. 25, 4877–4887.

Kirkpatrick, D., Denison, C., Gygi, S., 2005. Weighing in on ubiquitin: the expanding role of mass-spectrometry-based proteomics. Nat. Cell Biol. 7, 750–757.

Kurihara, L.J., Kikuchi, T., Wada, K., Tilghman, S.M., 2001. Loss of Uch-L1 and Uch-L3 leads to neurodegeneration, posterior paralysis and dysphagia. Hum. Mol. Genet. 10, 1963–1970.

Kurihara, L.J., Semenova, E., Levorse, J.M., Tilghman, S.M., 2000. Expression and functional analysis of Uch-L3 during mouse development. Mol. Cell Biol. 20, 2498–2504.

Kwon, J., Wang, Y.L., Setsuie, R., Sekiguchi, S., Sakurai, M., Sato, Y., Lee, W.W., Ishii, Y., Kyuwa, S., Noda, M., Wada, K., Yoshikawa, Y., 2004. Developmental regulation of ubiquitin C-terminal hydrolase isozyme expression during spermatogenesis in mice. Biol. Reprod. 71, 515–521.

Larsen, C.N., Krantz, B.A., Wilkinson, K.D., 1998. Substrate specificity of deubiquitinating enzymes: ubiquitin C-terminal hydrolases. Biochemistry 37, 3358–3368.

Larsen, C.N., Price, J.S., Wilkinson, K.D., 1996. Substrate binding and catalysis by ubiquitin C-terminal hydrolases: identification of two active site residues. Biochemistry 35, 6735–6744.

Leroy, E., Boyer, R., Auburger, G., Leube, B., Ulm, G., Mezey, E., Harta, G., Brownstein, M.J., Jonnalagada, S., Chernova, T., Dehejia, A., Lavedan, C., Gasser, T., Steinbach, P.J., Wilkinson, K.D., Polymeropoulos, M.H., 1998. The ubiquitin pathway in Parkinson's disease. Nature 395, 451–452.

Liu, Y., Fallon, L., Lashuel, H.A., Liu, Z., Lansbury Jr., P.T., 2002. The UCH-L1 gene encodes two opposing enzymatic activities that affect alpha-synuclein degradation and Parkinson's disease susceptibility. Cell 111, 209–218.

Manago, Y., Kanahori, Y., Shimada, A., Sato, A., Amano, T., Sato-Sano, Y., Setsuie, R., Sakurai, M., Aoki, S., Wang, Y.L., Osaka, H., Wada, K., Noda, M., 2005. Potentiation of ATP-induced currents due to the activation of P2X receptors by ubiquitin carboxy-terminal hydrolase L1. J. Neurochem. 92, 1061–1072.

Misaghi, S., Galardy, P.J., Meester, W.J., Ovaa, H., Ploegh, H.L., Gaudet, R., 2005. Structure of the ubiquitin hydrolase UCH-L3 complexed with a suicide substrate. J. Biol. Chem. 280, 1512–1520.

Mukhopadhyay, D., Riezman, H., 2007. Proteasome-independent functions of ubiquitin in endocytosis and signaling. Science 315, 201–205.

Nijman, S.M., Luna-Vargas, M.P., Velds, A., Brummelkamp, T.R., Dirac, A.M., Sixma, T.K., Bernards, R., 2005. A genomic and functional inventory of deubiquitinating enzymes. Cell 123, 773–786.

Nishikawa, K., Li, H., Kawamura, R., Osaka, H., Wang, Y.L., Hara, Y., Hirokawa, T., Manago, Y., Amano, T., Noda, M., Aoki, S., Wada, K., 2003. Alterations of structure and hydrolase activity of parkinsonism-associated human ubiquitin carboxyl-terminal hydrolase L1 variants. Biochem. Biophys. Res. Commun. 304, 176–183.

Ogawa, H., Ishiguro, K., Gaubatz, S., Livingston, D.M., Nakatani, Y., 2002. A complex with chromatin modifiers that occupies E2F- and Myc-responsive genes in G0 cells. Science 296, 1132–1136.

Osaka, H., Wang, Y.L., Takada, K., Takizawa, S., Setsuie, R., Li, H., Sato, Y., Nishikawa, K., Sun, Y.J., Sakurai, M., Harada, T., Hara, Y., Kimura, I., Chiba, S., Namikawa, K., Kiyama, H., Noda, M., Aoki, S., Wada, K., 2003. Ubiquitin carboxy-terminal hydrolase L1 binds to and stabilizes monoubiquitin in neuron. Hum. Mol. Genet. 12, 1945–1958.

Rubinsztein, D.C., 2006. The roles of intracellular protein-degradation pathways in neurodegeneration. Nature 443, 780–786.

Saigoh, K., Wang, Y.L., Suh, J.G., Yamanishi, T., Sakai, Y., Kiyosawa, H., Harada, T., Ichihara, N., Wakana, S., Kikuchi, T., Wada, K., 1999. Intragenic deletion in the gene encoding ubiquitin carboxy-terminal hydrolase in gad mice. Nat. Genet. 23, 47–51.

Sakurai, M., Ayukawa, K., Setsuie, R., Nishikawa, K., Hara, Y., Ohashi, H., Nishimoto, M., Abe, T., Kudo, Y., Sekiguchi, M., Sato, Y., Aoki, S., Noda, M., Wada, K., 2006. Ubiquitin C-terminal hydrolase L1 regulates the morphology of neural progenitor cells and modulates their differentiation. J. Cell Sci. 119, 162–171.

Sakurai, M., Sekiguchi, M., Zushida, K., Yamada, K., Nagamine, S., Kabuta, T., Wada, K., 2008. Reduction in memory in passive avoidance learning, exploratory behaviour and synaptic plasticity in mice with a spontaneous deletion in the ubiquitin C-terminal hydrolase L1 gene. Eur. J. Neurosci. 27, 691–701.

Sano, Y., Furuta, A., Setsuie, R., Kikuchi, H., Wang, Y.L., Sakurai, M., Kwon, J., Noda, M., Wada, K., 2006. Photoreceptor cell apoptosis in the retinal degeneration of Uchl3-deficient mice. Am. J. Pathol. 169, 132–141.

Semenova, E., Wang, X., Jablonski, M.M., Levorse, J., Tilghman, S.M., 2003. An engineered 800 kilobase deletion of Uchl3 and Lmo7 on mouse chromosome 14 causes defects in viability, postnatal growth and degeneration of muscle and retina. Hum. Mol. Genet. 12, 1301–1312.

Setsuie, R., Wada, K., 2007. The functions of UCH-L1 and its relation to neurodegenerative diseases. Neurochem. Int. 51, 105–111.

Setsuie, R., Wang, Y.L., Mochizuki, H., Osaka, H., Hayakawa, H., Ichihara, N., Li, H., Furuta, A., Sano, Y., Sun, Y.J., Kwon, J., Kabuta, T., Yoshimi, K., Aoki, S., Mizuno, Y., Noda, M., Wada, K., 2007. Dopaminergic neuronal loss in transgenic mice expressing the Parkinson's disease-associated UCH-L1 I93M mutant. Neurochem. Int. 50, 119–129.

Todaro, G.J., Green, H., 1963. Quantitative studies of the growth of mouse embryo cells in culture and their development into established lines. J. Cell. Biol. 17, 299–313.

van Nocker, S., Vierstra, R.D., 1993. Multiubiquitin chains linked through lysine 48 are abundant in vivo and are competent intermediates in the ubiquitin proteolytic pathway. J. Biol. Chem. 268, 24766–24773.

Wada, H., Kito, K., Caskey, L.S., Yeh, E.T., Kamitani, T., 1998. Cleavage of the C-terminus of NEDD8 by UCH-L3. Biochem. Biophys. Res. Commun. 251, 688–692.

Walters, B., Campbell, S., Chen, P., Taylor, A., Schroeder, D., Dobrunz, L., Artavanistsakonas, K., Ploegh, H., Wilson, J., Cox, G., 2008. Differential effects of Usp14

Please cite this article in press as: Setsuie, R., et al., Ubiquitin dimers control the hydrolase activity of UCH-L3. Neurochem. Int. (2009), doi:10.1016/j.neuint.2008.12.013

and Uch-L1 on the ubiquitin proteasome system and synaptic activity. Mol. Cell. Neurosci. 45.

Wilkinson, K.D., 1997. Regulation of ubiquitin-dependent processes by deubiquitinating enzymes. Faseb J. 11, 1245–1256.

Wilkinson, K.D., Laleli-Sahin, E., Urbauer, J., Larsen, C.N., Shih, G.H., Haas, A.L., Walsh, S.T., Wand, A.J., 1999. The binding site for UCH-L3 on ubiquitin: mutagenesis and NMR studies on the complex between ubiquitin and UCH-L3. J. Mol. Biol. 291, 1067–1077.

Wilkinson, K.D., Lee, K.M., Deshpande, S., Duerksen-Hughes, P., Boss, J.M., Pohl, J., 1989. The neuron-specific protein PGP 9.5 is a ubiquitin carboxyl-terminal hydrolase. Science 246, 670–673.

Wood, M., Kaplan, M., Brensinger, C., Guo, W., Abel, T., 2005. Ubiquitin C-terminal hydrolase L3 (Uchl3) is involved in working memory. Hippocampus 15, 610–621.

Yin, L., Krantz, B., Russell, N.S., Deshpande, S., Wilkinson, K.D., 2000. Nonhydrolyzable diubiquitin analogues are inhibitors of ubiquitin conjugation and deconjugation. Biochemistry 39, 10001–10010.

Please cite this article in press as: Setsuie, R., et al., Ubiquitin dimers control the hydrolase activity of UCH-L3. Neurochem. Int. (2009), doi:10.1016/j.neuint.2008.12.013

Journal of
Nanoscience and Nanotechnology
Vol. 9, 670–672, 2009

Two-Photon Excitation Behavior of Thiophene-Based Oligomers and a Polymer

Takakazu Yamamoto[1,*], Akira Kumagai[1], Kenta Saito[2], and Takeharu Nagai[2,*]

[1] *Chemical Resources Laboratory, Tokyo Institute of Technology, 4259 Nagatsuta, Midori-ku, Yokohama 226-8503, Japan*
[2] *Research Institute for Electronic Science, Hokkaido University, Sapporo 001-0020, Japan*

The two-photon excitation action cross-sections of four kinds of co-oligomers of thiophene and pyridine (e.g., Py-(Th)$_n$-Py; Py = 2-pyridyl, Th = thiophene-2,5-diyl; n = 3, 4) and a copolymer constituted of alternating pyridazine and 4,4′-dihexyl- 2,2′-bithiophene units have been measured by using a reported value (σ_{2PE} at 780 nm = 10 GM) of green fluorescent protein as the reference. The co-oligomers give σ_{2PE} values of 14–26 GM and the copolymer shows σ_{2PE} of 23 GM.

Keywords: π-Conjugated Polymer, Oligomer, Two-Photone Excitation.

COMMUNICATION

Two-photon absorption phenomena are the subject of recent many papers.[1–8] One of the important applications is two-photon excitation of fluorescent molecules within deep inside living tissue. In combination with FRET (fluorescence resonance energy transfer)-based indicators, protein–protein interactions and activities of biomolecules are visualized.[8,9] Another application is the use as a light source for micro-fabrication to make, for example, three dimensional photonic crystals.[10] By the way, π-conjugated oligomers and polymers are also the subject of recent interest,[11–14] and two-photon absorption data of π-conjugated oligomers and polymers are expected to give information about fundamental electronic states of the oligomers and polymers.

Recently we reported synthesis of the following π-conjugated co-oligomers and copolymer[15,16] with an intramolecular charge transferred (CT) electronic structure. In the co-oligomers and copolymer, thiophene is an electron-donating unit, whereas pyridine and pyridazine are electron-accepting units.[15,16] For these co-oligomers and copolymer we have studied their two-photon absorption behavior.

We herein report the obtained results. The two-photon absorption data were acquired by irradiation of solutions of the co-oligomers and copolymer with 780 nm laser. According to the one photon absorption spectrum of the tested dyes, we used 780 nm laser as the light source for two-photon excitation.

The co-oligomers **1**–**6** (Ref. [15]) and the copolymer P(PydTh) (R = hexyl)[16] were prepared according to the literature. α-Sexithiophene (α-Th$_6$) was purchased from Tokyo Kasei Co. Ltd. Fluorescence spectra were recorded on a Hitachi F-4010 spectrometer. Quantum yield (Φ) of fluorescence was calculated using a quinine sulfate standard (ca. 10^{-5} M solution in 0.5 M H_2SO_4 with Φ = 54.6%[17]). Two-photon excitation was carried out under an inverted microscopy (Olympus FV-300) equipped with an Olympus 20× NA0.75 objective lens. 780 nm pulse laser (Maitai, Spectra Physics) was irradiated to the sample solution in the two-photon excitation, and intensity of the laser was adjusted by a computer controlled AOTF (acousto-optical tunable filter) system. Fluorescence intensity in a region of interest was measured. Florescence intensity of pure chloroform did not show dependence on the intensity of the laser. mSEGFP, a variant of green fluorescent protein with mutations in EGFP (M153T, V163A, S175G and A206K), was used as the standard for determination of the cross section (σ_{2PE}) of the two-photon absorption (σ_{2PE} of mSEGFP = 10 GM (1 GM = 10^{-50} cm^4 s/photon)[7,18]). Co-oligomers **1**–**6** were dissolved in DMSO (dimethyl sulfoxide), and P(PydTh) (6.5 mg) was dissolved in 8.0 mL of xylene at 100 °C. Most part of P(PydTh) was dissolved in xylene, however, there was some insoluble part. The insoluble part was removed by filtration.

Figure 1 shows dependence of the fluorescence intensity of the co-oligomers **3**–**6** and α-Th$_6$ on the intensity of irradiated laser at 780 nm. Solutions of these co-oligomers and α-Th$_6$ show the UV-vis absorption peak in a range of about 380–440 nm,[15] and they are essentially transparent at 780 nm. The co-oligomers 1 and 2 with a shorter

*Authors to whom correspondence should be addressed.

1533-4880/2009/9/670/003 doi:10.1166/jnn.2009.J070